ACADÉMIE
DES SCIENCES
INSTITUT DE FRANCE

Comptes Rendus
Physique

Iacopo Carusotto

How to exploit driving and dissipation to stabilize and manipulate quantum many-body states

Volume 26 (2025), p. 533-569

Online since: 15 September 2025

https://doi.org/10.5802/crphys.258

This article is licensed under the
Creative Commons Attribution 4.0 International License.
http://creativecommons.org/licenses/by/4.0/

The Comptes Rendus. Physique *are a member of the Mersenne Center for open scientific publishing*
www.centre-mersenne.org — e-ISSN : 1878-1535

ACADÉMIE DES SCIENCES
INSTITUT DE FRANCE

Comptes Rendus. Physique
2025, Vol. 26, p. 533-569
https://doi.org/10.5802/crphys.258

Intervention in a conference / *Intervention en colloque*

How to exploit driving and dissipation to stabilize and manipulate quantum many-body states

Comment tirer parti du pompage et de la dissipation pour stabiliser et manipuler des états quantiques à N corps

Iacopo Carusotto[a]

[a] Pitaevskii BEC Center, INO-CNR and Dipartimento di Fisica, University of Trento, Italy
E-mail: iacopo.carusotto@ino.cnr.it

Abstract. We give a pedagogical introduction to the basic concepts of quantum fluids of light and to the different techniques that are being developed to exploit driving and dissipation to stabilize and manipulate interesting many-body states in quantum fluids of light in cavity configurations. In the weakly interacting regime, this approach has allowed to study, among others, superfluid light, nonequilibrium Bose–Einstein condensation, photonic analogs of Hall effects, and is opening the way towards the realization of a new family of analog models of gravity. In the strongly interacting regime, the recent observations of Mott insulators and baby Laughlin fluids of light are opening promising avenues towards the study of novel strongly correlated many-body states.

Résumé. Nous donnons une introduction pédagogique aux concepts de base des fluides quantiques de lumière et aux différentes techniques qui ont été développées pour exploiter le pompage et la dissipation afin de stabiliser et de manipuler des états à N corps intéressants dans des fluides quantiques de lumière en cavité. Dans le régime d'interaction faible, cette approche a permis d'étudier, entre autres, la lumière superfluide, la condensation de Bose–Einstein hors d'équilibre, les analogues photoniques des effets Hall, et ouvre la voie à la réalisation d'une nouvelle famille de modèles analogiques de la gravité. Dans le régime d'interaction forte, les observations récentes d'isolants de Mott et de tout petits fluides de Laughlin faits de lumière ouvrent des voies prometteuses pour l'étude de nouveaux états à N corps fortement corrélés.

Keywords. Driven-dissipative systems, many-body problem, nonequilibrium statistical mechanics, strongly correlated quantum fluids, quantum fluids of light.

Mots-clés. Systèmes dissipatifs pompés, problème à N corps, mécanique statistique hors d'équilibre, fluides quantiques fortement corrélés, fluides quantiques de lumière.

Funding. We acknowledge financial support by: Provincia Autonoma di Trento (PAT); from Q@TN, the joint lab between University of Trento, FBK-Fondazione Bruno Kessler, INFN-National Institute for Nuclear Physics and CNR-National Research Council; the National Quantum Science and Technology Institute through the PNRR MUR Project under grant PE0000023-NQSTI, co-funded by the European Union — NextGeneration EU; the Deutsche Forschungsgemeinschaft (DFG, German Research Foundation) via the Research Unit FOR 5688 "Driven-dissipative many-body systems of ultracold atoms", project number 521530974.

Manuscript received 18 March 2025, revised 3 July 2025, accepted 16 July 2025.

1. Introduction

In the last decades, a most promising platform for many-body physics has emerged thanks to the dramatic advances in the laser cooling techniques for dilute atomic gases. This has allowed to reach unprecedented temperatures in the sub-nanokelvin range and has allowed the clean observation of textbook many-body phenomena such as Bose–Einstein condensation (BEC), the crossover from BEC to a Bardeen–Cooper–Schrieffer (BCS) superconductive state of Fermi gases, and first realizations of strongly interacting states of matter such as Mott insulators and fractional quantum Hall fluids [1–4]. As compared to traditional condensed matter systems which are subject to sizable fabrication disorder and spurious additional effects, atomic gases enjoy an extraordinary level of cleanness and control at the microscopic level, which permits a quantitative comparison with ab initio theoretical calculations. Still, the available values of the temperature are typically still too high to observe the most exciting strongly correlated states of matter.

More or less in the same years, the merging of ideas from quantum optics and many-body physics has led to the development of the concept of fluid of light, namely an assembly of photons confined in suitable cavity devices where they display a finite effective mass and sizable interactions mediated by the optical nonlinearity of the medium [5]. As a result of these features, the photon gas starts displaying the typical collective properties of a standard quantum fluid such as superfluidity and condensation and, by now, an active research is being devoted to the quest for strongly correlated states of the fluid of light [6,7]. As a key difference compared to atomic gases, fluids of light in cavity configurations are typically characterized by a driven-dissipative nature, where the state of the fluid is not determined by a thermal equilibrium condition, but rather by a dynamical balance of pumping and losses [8,9].

This was initially considered as a serious drawback, as it made it difficult to realize the most celebrated textbook models of many-body physics. But over the years it has become clear that the nonequilibrium nature of the fluid opens the way to new physical phenomena and offers a wide variety of novel experimental tools for the stabilization, the manipulation and the diagnostics of the fluid. In particular, very different states of matter can be realized by simply tuning the properties of the laser beams used to generate the fluid of light. As the open nature of the fluid of light naturally provides a way to exchange energy and particles with the external world, it can be exploited to reduce the level of thermal-like excitation of the fluid. Rather than trying to cool the system towards lower and lower temperatures, the idea is then to design driving and loss mechanisms that autonomously stabilize the system into the desired quantum many-body state.

Quite interestingly, these efforts in the nonequilibrium stabilization of fluids of light go on par with analogous developments in the context of cold atoms aiming at exploiting driving and dissipation to stabilize interesting many-body states of atomic matter [10–12], also coupled to optical cavities [13–15]. As a key difference, however, the typical dissipation schemes considered for atoms do not involve a net flux of atoms through the system from/to external reservoirs. Stimulated by recent pioneering experiments [16–18], it will be an exciting new frontier to explore the new nonequilibrium physics of driven-dissipative cold atomic gases that can exchange particles with one or more external reservoirs.

The goal of this article is to summarize the main ideas in the physics of fluids of light in cavity configurations and introduce the reader to the different strategies that have been developed in this context for the driven-dissipative stabilization of different quantum many-body states. As several reviews are already available on this topic [5–9], our focus will be on a pedagogical presentation of the main theoretical tools that can be used to describe the system under different pumping conditions and to design schemes to exploit the driven-dissipative nature for novel investigations of many-body physics. A brief discussion of some specific experiments will also

be given, yet without the ambition of providing a complete bibliography on this wide and active field of research. In particular, we will not dwell into the active research that is going on in fluids of light in propagating geometries [19] and which has already led to a number of recent landmark experiments, ranging from superfluidity features [20,21], quantized vortices [22–24], turbulent [25,26] and condensation phenomena [27–29], to the quantum dynamics past quenches [30] and pioneering work on strongly interacting gases [31,32]. As the quantum dynamics of the propagating fluid of light is an essentially conservative one, this area of research is somehow disconnected from the driven-dissipative dynamics of cavity configurations that is the focus of the present article.

In spite of these limitations, we hope that our presentation will be useful to those researchers that wish to export ideas of quantum fluids of light into the field of cold atoms, so as to realize driven-dissipative schemes that autonomously stabilize strongly correlated states of matter in ultracold atomic gases. The structure of the article is the following. In Section 2 we give the basic concepts in the field of fluids of light and we summarize the basic blocks of their theoretical description. Section 3 is focussed to the regime of weakly interacting fluids where a mean-field theory provides an accurate description of the system: after a brief summary of the theoretical description, we will outline a few specific configurations where the driven-dissipative nature of the fluid of light opens new exciting possibilities of stabilizing and manipulating many-body states and gives rise to interesting new effects. In Section 4, we turn to strongly interacting systems, with a special attention being paid to the stabilization and the manipulation of driven-dissipative fractional quantum Hall states. In Section 5 we give our conclusions and we sketch our vision of the perspectives of this field, with a special emphasis on transferring ideas of quantum fluids of light back to atomic gases in novel driven-dissipative regimes.

2. Basic concepts of quantum fluids of light

In our intuitive picture, we are used to associate light to propagating electromagnetic waves or, in a quantum description, to a stream of corpuscular photons that travel across space at a very fast speed. The concept of *Quantum Fluid of Light (QFL)* defies this picture. Merging ideas from condensed matter physics and optics, it deals with the collective behaviours that assemblies of photons display when they are endowed of an effective mass and sizable inter-particle interactions [5] and are then manipulated as a standard fluid of many interacting particles.

This section starts with a brief review of these basic concepts and, then, elaborates on the intrinsically driven-dissipative nature of the fluid of light in cavity configurations and on the tools that are needed for its theoretical description.

2.1. *Conservative dynamics*

2.1.1. *Photon mass in cavity configurations*

Within special relativity, massless particles travel at a constant speed c and a finite mass is required to put particles at rest. In vacuo, the photons that constitute light beams are massless particles. The situation can dramatically change in spatially confined geometries, where photons acquire a finite effective mass for their motion along some dimensions thanks to the spatial confinement along the other dimensions.

The simplest case is the one sketched in the top panel of Figure 1, namely a cavity enclosed by a pair of plane-parallel metallic mirrors located along the xy plane and separated by a distance L_z along z. As the tangential component of the electric field has to vanish at the metallic mirrors, the z component of the wavevector is quantized as $k_z^{(q)} = \pi q / L_z$ according to the positive integer

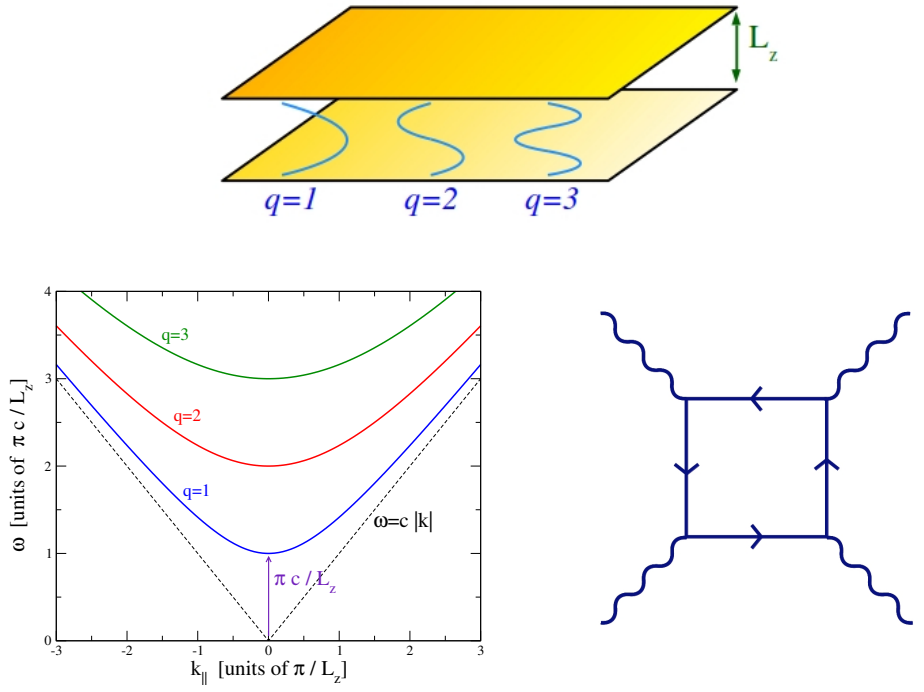

Figure 1. Light confinement in a planar microcavity (top) results in a relativistic dispersion for the in-plane motion of photons (bottom left). Feynman diagram describing the Heisenberg–Euler photon-photon interaction processes mediated by virtual electron-positron pairs in Quantum Electrodynamics (bottom right).

number $q > 0$ characterizing the number of field nodes along the z direction. On the other hand, given the translational symmetry along the xy plane, the motion along these directions is free and the corresponding component $\mathbf{k}_\parallel$ of the wavevector can have arbitrary values.

As a result, forgetting for simplicity the polarization degrees of freedom, electromagnetic waves in a planar cavity filled of a material of refractive index n can be described in terms of a massive relativistic-like dispersion,

$$\left(\hbar\omega^{(q)}(\mathbf{k}_\parallel)\right)^2 = (m^{(q)}c^2)^2 + \frac{\hbar^2 c^2}{n^2}\mathbf{k}_\parallel^2, \tag{1}$$

where the finite effective mass of each q branch

$$m^{(q)}c^2 = \frac{\hbar c k_z^{(q)}}{n} = \hbar\omega_o^{(q)} \tag{2}$$

arises from the zero-point confinement along z and grows with the quantum number q. As usual in special relativity, the mass parameter $m^{(q)}$ encodes both a *rest mass* related to the energy $\hbar\omega_o^{(q)}$ of a photon at rest in the zero-momentum $\mathbf{k}_\parallel = 0$ state and a *kinetic mass* related to growth of the energy of a photon when this is set into motion at a non-zero $\mathbf{k}_\parallel$. In the bottom left panel of Figure 1, the former can be read out as the energy gap below the dispersion, while the latter gives the curvature of the dispersion around its bottom.

Under a non-relativistic approximation, a parabolic form of the dispersion is obtained for each q branch at small in-plane momenta,

$$\omega^{(q)}(\mathbf{k}_\parallel) \simeq \omega_o^{(q)} + \frac{\hbar}{2m^{(q)}}\,\mathbf{k}_\parallel^2. \tag{3}$$

Upon quantization, the electric field in the cavity can be expanded as

$$\widehat{E}(\mathbf{r}_\parallel, z) = \sum_{q=1}^{\infty} \mathscr{E}_q(z)\,\widehat{\Psi}_q(\mathbf{r}_\parallel) + \mathscr{E}_q^*(z)\,\widehat{\Psi}_q^\dagger(\mathbf{r}_\parallel) \tag{4}$$

in terms of a set of quantum field operators $\widehat{\Psi}_q(\mathbf{r}_\parallel)$ describing each q branch and satisfying bosonic commutation rules,

$$\left[\widehat{\Psi}_q(\mathbf{r}_\parallel), \widehat{\Psi}_{q'}^\dagger(\mathbf{r}'_\parallel)\right] = \delta_{q,q'}\,\delta^{(2)}(\mathbf{r}_\parallel, \mathbf{r}'_\parallel). \tag{5}$$

The wavefunction of mode q around the bottom of the branch

$$\mathscr{E}_q(z) = \sqrt{\frac{4\pi\hbar\omega_o^{(q)}}{n^2 L}}\,\sin\!\left(\frac{\pi\, q\, z}{L}\right) \tag{6}$$

displays nodes at $z = 0, L$ and gives an energy $\hbar\omega_o^{(q)}$ per photon.

The form (3) of the dispersion suggests a straightforward way to generate an external potential for photons. Replacing in (3) the explicit dependence of $\omega_o^{(q)}$ on the cavity parameters (2), it is in fact immediate to see how a slow lateral dependence of the refractive index $n(\mathbf{r}_\parallel)$ and/or of the cavity thickness $L(\mathbf{r}_\parallel)$ can be exploited to generate an effective in-plane potential profile

$$V^{(q)}(\mathbf{r}_\parallel) = \omega_o^{(q)}(\mathbf{r}_\parallel) = \frac{c\pi q}{n(\mathbf{r}_\parallel)\,L(\mathbf{r}_\parallel)}. \tag{7}$$

Such a potential can be used, e.g., to exert uniform forces in the case of a uniform gradient or to localize the photons in suitably defined potential wells. Of course, in order to avoid introducing undesired losses due to the abrupt in-plane variation of the field mode, the $\mathbf{r}_\parallel$-dependence of L and n has to be sufficiently smooth to avoid non-adiabatic inter-branch transitions.

Even though these simple formulas have been obtained for the simplest case of metallic cavities, qualitatively similar results hold for other kinds of planar microcavities with translational symmetry along the xy plane, in particular semiconductor DBR microcavities enclosed by distributed Bragg reflectors [5,33].

2.1.2. *Photon-photon interactions*

A superposition principle for light fields directly follows from the linearity of the classical Maxwell equations in vacuo [34]: two light beams propagate independently of each other, and a light beam cannot be used to modify the propagation of another beam. Quite remarkably, this cornerstone of classical electrodynamics ceases to be true in quantum electrodynamics where photons can be converted into electron-positron pairs and back.

Among a plethora of other effects, this interaction vertex results into the effective photon-photon interaction process first pointed out by Heisenberg and Euler in the 1930's [35] and illustrated in the bottom right panel of Figure 1. As this process is mediated by the creation of virtual electron-positron pairs, the effective scattering cross section is only significant for high energy photons of energies comparable to the electron/positron rest mass of around 0.5 MeV, while it is dramatically suppressed at lower energies according to

$$\sigma \propto \alpha^4 \left(\frac{h}{m_{el}c}\right)^2 \left(\frac{\hbar\omega}{m_{el}c^2}\right)^6. \tag{8}$$

In addition to the squared electron Compton wavelength $h/(m_e c) \simeq 2.4$ pm and the four fine-structure $\alpha = e^2/\hbar c \sim 1/137$ factors corresponding to the four interaction vertices, the main suppression comes from the detuning of the virtual intermediate states due to the large rest mass of the virtual electron-positron pairs compared to the incident photon energy. For visible light in the eV range, this suppression factor can be as huge as 10^{-36} making the observation of Heisenberg–Euler photon-photon scattering processes in table-top experiments very difficult. Efforts are in progress to observe photon-photon scattering in vacuo using strong laser beams [36] or γ-rays [37–39] and experimental results have been reported for a related effect of photons scattering off the strong electrostatic field surrounding a heavy-ion [40].

The microscopic mechanism of photon-photon scattering in vacuo suggests that a huge reinforcement of the effect would be obtained if lighter particles were available as intermediate states of the scattering process. This naturally occurs in solid-state insulating materials, whose ground state consists of a filled valence band and an empty conduction band. Promoting an electron from the valence to the conduction band can be reinterpreted as the creation of an electron in the conduction band and a hole in the valence band [41]. The energy cost of this process is roughly determined by the electronic energy gap of the material, typically in the eV range. A naive translation of this result into the formula (8) predicts a dramatic reinforcement of the photon-photon scattering cross section by a factor of the order 10^{36} and suggests the actual observability of photon-photon collision processes in material media.

This intuitive picture of photon-photon collisions can be put on solid grounds in the framework of nonlinear optics [42,43]: here, binary photon-photon interactions are encoded in the $\chi^{(3)}$ optical nonlinearity of the medium, which describes a dielectric polarization proportional to the cube of the applied electric field. Such nonlinear optical processes occur in generic optical media and strong efforts are presently being paid to realize materials where the strength of the optical nonlinearities is reinforced well beyond the prediction of a naive extension of (8). Among the most promising platforms for this purpose, we can mention superconductor-based circuit-QED devices operating in the microwave range [7,44] or optically dressed atomic gases in the so-called Rydberg-EIT configurations [6,31,32]: such exceptional media are at the heart of the recent developments towards the realization of strongly interacting photon fluids that we are going to present later on in Section 4.

For the sake of simplicity, we will restrict our quantitative discussion of the photon-photon interaction Hamiltonian to a simplest case that can be worked out in analytical terms. We model photon-photon interactions as a normally-ordered, spatially local quartic term of the form

$$H_{\rm int} = \frac{\hbar g_{\rm 3d}}{2} \int {\rm d}^3\mathbf{r} : \widehat{E}(\mathbf{r})^4 : \tag{9}$$

By equating[1] the nonlinear frequency shift predicted by the Hamiltonian (9) for a given plane-wave mode at $\mathbf{k}$ in a spatially uniform geometry when only this mode is coherently occupied with amplitude $\overline{\alpha}$,

$$\delta\omega = 6 g_{\rm 3d} \, |\mathscr{E}|^4 \, |\overline{\alpha}|^2 \tag{10}$$

with the amplitude of the nonlinear polarization at the frequency of the mode predicted by the nonlinear optics formalism,

$$P_{\rm nl} = 3\chi^{(3)} \, |\mathscr{E}|^2 \mathscr{E} \, |\overline{\alpha}|^2 \, \overline{\alpha}, \tag{11}$$

we obtain that

$$g_{\rm 3d} = -\frac{\chi^{(3)}}{2\hbar}. \tag{12}$$

[1] We have assumed a spatio-temporally local nonlinearity, so the total nonlinear polarization is $P_{\rm nl}^{\rm (tot)}(\mathbf{r},t) = \chi^{(3)} \, E^3(\mathbf{r},t)$. The uniform-space mode normalization is $\mathscr{E} = (2\pi\hbar\omega/n^2)^{1/2}$. The amplitude of the coherent state is normalized as $\langle \hat{a}_{\mathbf{k}} \rangle = (2\pi)^3 \, \delta(\mathbf{k}-\mathbf{k}') \, \overline{\alpha}$.

Moving to a planar cavity geometry completely filled by the nonlinear medium and restricting our attention to the lowest $q = 1$ mode, we can insert the explicit expression for the cavity mode profile (6) into (9) and integrate over z, so that we obtain a nonlinear interaction term of the usual form

$$H_{\rm int} = \frac{\hbar g_{\rm nl}}{2} \int {\rm d}^2\mathbf{r}_\parallel \, \widehat{\Psi}^\dagger(\mathbf{r}_\parallel)\, \widehat{\Psi}^\dagger(\mathbf{r}_\parallel)\, \widehat{\Psi}(\mathbf{r}_\parallel)\, \widehat{\Psi}(\mathbf{r}_\parallel) \tag{13}$$

with an interaction strength $g_{\rm nl}$ that is related to the third-order nonlinear susceptibility $\chi^{(3)}$ of the medium by [45]

$$g_{\rm nl} = -\frac{18\pi^2(\hbar\omega_o)^2}{n^4 L}\,\chi^{(3)}. \tag{14}$$

2.1.3. *The Hamiltonian*

Putting all these effects together, the dynamics of the quantum fluid of light in the lowest energy states around the bottom of the $q = 1$ branch can be summarized by the following bosonic Hamiltonian [5]:

$$H = \int {\rm d}^2\mathbf{r}_\parallel \left[\hbar\omega_o \widehat{\Psi}^\dagger(\mathbf{r}_\parallel)\, \widehat{\Psi}(\mathbf{r}_\parallel) + \frac{\hbar^2}{2m^*} \nabla_\parallel \widehat{\Psi}^\dagger(\mathbf{r}_\parallel)\, \nabla_\parallel \widehat{\Psi}(\mathbf{r}_\parallel) + \hbar V(\mathbf{r}_\parallel)\, \widehat{\Psi}^\dagger(\mathbf{r}_\parallel)\, \widehat{\Psi}(\mathbf{r}_\parallel) + \right.$$
$$\left. + \frac{\hbar g_{\rm nl}}{2} \widehat{\Psi}^\dagger(\mathbf{r}_\parallel)\, \widehat{\Psi}^\dagger(\mathbf{r}_\parallel)\, \widehat{\Psi}(\mathbf{r}_\parallel)\, \widehat{\Psi}(\mathbf{r}_\parallel) \right]. \tag{15}$$

Here, the first and second terms respectively describe the rest energy of the photons and their (nom-relativistic) in-plane kinetic energy, as defined in (1)–(2). The third term models the external potential (7) acting on the photons and the fourth one accounts for the (contact) photon-photon interactions mediated by the optical nonlinearity (14). All together, it is immediate to recognize this Hamiltonian exactly corresponds to the one of a bosonic gas of material particles, in particular of ultracold atoms [1].

2.2. *Driving and dissipation*

In contrast to fluids of material particles where the lifetime of the microscopic constituents is typically very long compared to the many-body dynamics of interest, photons in the typical cavity devices used for experiments on quantum fluids of light experience a significant decay rate, due to a combination of non-radiative losses by absorption processes in the cavity material and radiative ones through the cavity mirrors.

Two philosophies are then available to deal with these processes. On one hand, a part of the community is making strong efforts to improve the cavity design to maximize the lifetime and, in this way, the time-window available for the conservative many-body dynamics. In addition to the optimized planar microcavity devices used to study quasi-equilibrium Bose–Einstein condensation effects in polariton fluids [46,47], such a strategy is implicitly undertaken in many experiments addressing the many-body physics of microwave photons in superconductor-based circuit-QED platforms [48–50].

On the other hand, one can try to *turn a bug into a feature* and exploit the driven-dissipative nature of the fluid of light to explore the new physics that arises from the interplay of driving and dissipation with the conservative many-body dynamics. Some external pump is in fact needed to overcome the effect of losses that would normally tend to dissipate the fluid: rather than considering it just as an experimental complication, the presence of the pump opens a range of new possibilities to manipulate the many-body state of the fluid. On top of this, one must not forget that radiative losses transfer all properties of the in-cavity field to the emitted light [51], so that the quantum state of the fluid of light can be reconstructed in real time just by looking at the quantum optical properties of the emitted radiation. As we are going to see in what follows,

these are crucial advantages of fluids of light as compared to, e.g., ultracold atomic systems where experiments often require destructive imaging techniques.

Before dwelling into this rich physics, it is important to complete the theoretical framework by discussing how the driving and dissipation processes can be included into the theoretical model. This will be the subject of the next subsections.

2.2.1. *Losses*

Losses in usual devices are linear in the field amplitude and have an approximately frequency- and wavevector-independent rate, so that they can be described at the level of the master equation for the density operator

$$\frac{\mathrm{d}\widehat{\rho}}{\mathrm{d}t} = -\frac{i}{\hbar}[H,\widehat{\rho}] + \mathscr{L}[\widehat{\rho}] \tag{16}$$

by Markovian Lindblad terms of the form

$$\mathscr{L}_{\rm loss}[\widehat{\rho}] = \frac{\gamma_{\rm loss}}{2}\int \mathrm{d}^2\mathbf{r}_\parallel \left[2\widehat{\Psi}(\mathbf{r}_\parallel)\,\widehat{\rho}\,\widehat{\Psi}^\dagger(\mathbf{r}_\parallel) - \widehat{\Psi}^\dagger(\mathbf{r}_\parallel)\,\widehat{\Psi}(\mathbf{r}_\parallel)\,\widehat{\rho} - \widehat{\rho}\,\widehat{\Psi}^\dagger(\mathbf{r}_\parallel)\,\widehat{\Psi}(\mathbf{r}_\parallel)\right]. \tag{17}$$

While this theory is sufficient to deal with typical experimental configurations with moderate to long photon lifetimes, one must not forget that some extra care has to be paid if the loss rate is comparable to the frequency of the cavity mode and/or one is operating in the so-called ultrastrong light-matter coupling regime where the quantum vacuum state of the cavity is strongly distorted from the usual QED vacuum: in this case, non-Markovian terms are often needed to avoid unphysical *perpetuum mobile* behaviours in the theory [52–54]. As the cavities that are typically used for quantum fluid of light experiments are far from this regime, in what follows we will safely stick to the form (17) of the loss term.

2.2.2. *Coherent pump*

The coherent pumping associated to the injection of photons by a coherent field incident on the cavity mirror can be described within the input-output formalism [51,55] by additional terms in the conservative Hamiltonian. In the simplest case where the transmission amplitude η of the cavity mirror is flat in both frequency and wavevector, these have the simple form

$$H_{\rm coh} = \int \mathrm{d}^2\mathbf{r}_\parallel \left[\hbar\eta\,\mathscr{E}_{\rm inc}(\mathbf{r}_\parallel,t)\,\widehat{\Psi}^\dagger(\mathbf{r}_\parallel) + \hbar\eta^*\,\mathscr{E}^*_{\rm inc}(\mathbf{r}_\parallel,t)\,\widehat{\Psi}(\mathbf{r}_\parallel)\right] \tag{18}$$

in terms of the (fully arbitrary) space- and time-dependent amplitude of the incident field $\mathscr{E}_{\rm inc}(\mathbf{r}_\parallel,t)$ at the cavity mirror location.

While this formulation is sufficient to deal with the typical microcavity devices used in quantum fluid of light experiments, more complicated situations can be described by replacing the constant mirror transmission amplitude η with a convolution with a spatio-temporal kernel $\eta(\mathbf{r}_\parallel,t)$ to account for the frequency- and wavevector-dependence of the mirror transmission amplitude. As usual in the input-output theory, such a generalized form of the transmission amplitude must be associated to a corresponding frequency and wavevector dependence of the radiative loss rate [53].

2.2.3. *Incoherent pump*

Incoherent pumping terms originate from an incident thermal radiation or from spontaneous emission processes by some suitably excited medium embedded in the cavity. This can consist, e.g., of population-inverted two-level systems or of an electrically-injected electron-hole gas. In contrast to the coherent pumping described in (18), such incoherent processes are totally phase-insensitive and do not inherit any coherence from the electric/optical mechanism used to excite the two-level systems or inject the electron-hole gas. While coherent pumping processes may

induce reversible oscillatory Rabi-flopping dynamics, incoherent pumping is characterized by an intrinsic irreversible push towards the excited states.

At a simplest level of approximation, one may be tempted to describe the effect of incoherent pumping within a Born and Markov approximation by including a Lindblad term of the form

$$\mathscr{L}_{\rm pump}[\widehat{\rho}] = \frac{\gamma_{\rm pump}}{2}\int {\rm d}^2\mathbf{r}_\parallel \left[2\widehat{\Psi}^\dagger(\mathbf{r}_\parallel)\,\widehat{\rho}\,\widehat{\Psi}(\mathbf{r}_\parallel) - \widehat{\Psi}(\mathbf{r}_\parallel)\,\widehat{\Psi}^\dagger(\mathbf{r}_\parallel)\,\widehat{\rho} - \widehat{\rho}\,\widehat{\Psi}(\mathbf{r}_\parallel)\,\widehat{\Psi}^\dagger(\mathbf{r}_\parallel)\right] \tag{19}$$

into the master equation (16). This is a good approximation as long as the gain has a broadband nature and, more importantly, the pump rate remains below the loss rate $\gamma_{\rm pump} < \gamma_{\rm loss}$. In this regime, the effect of incoherent pumping is to sporadically inject some extra photon into the cavity, which is then rapidly lost: in addition to spontaneous processes injecting photons (almost) uniformly into all modes of the cavity, incoherent emission processes may also enjoy bosonic stimulation so the emission will be reinforced into those cavity modes that already contain photons.

On the other hand, a most interesting physics occurs when incoherent pumping overcomes losses and a coherent fluid of light is spontaneously generated in the cavity via a nonequilibrium condensation mechanism analogous to lasing [8]: in this case, a naive use of (19) would lead to a divergence of the in-cavity field amplitude so an accurate description of the steady-state of the in-plane cavity field requires including gain saturation effects.

2.2.4. *Gain saturation & frequency selectivity*

A common strategy to account for gain saturation is to explicitly include the microscopic dynamics of the emission process into the quantum theoretical description. Such an approach dates back to early works in laser theory [56,57], where the emitters are described as two-level systems driven in a population-inverted state by some external incoherent pumping.

In a simplest geometry where the field is discretized in a lattice of cavities each supporting a single optical mode and embedding a single two-level emitter, the local Hamiltonian of each site (to be supplemented by hopping terms in a full lattice model) has the form

$$H_{\rm site} = \hbar\omega_0\,\widehat{a}^\dagger\widehat{a} + \hbar\omega_{\rm em}\,\widehat{\sigma}_z + \hbar\Omega_R\left[\widehat{a}^\dagger\widehat{\sigma}^- + \widehat{a}\widehat{\sigma}^+\right] \tag{20}$$

where the bosonic $\widehat{a}$ and the spin $\sigma^{z,\pm}$ operators respectively describe the photonic field (of natural frequency ω_0) and the two-level emitter (of natural frequency $\omega_{\rm em}$). The population inversion is enforced by an incoherent pumping acting on the emitter, as described by a Lindblad term of the form

$$\mathscr{L}_{\text{pump-em}}[\widehat{\rho}] = \frac{\Gamma_{\rm P}}{2}\left[2\widehat{\sigma}^+\widehat{\rho}\widehat{\sigma}^- - \widehat{\sigma}^-\widehat{\sigma}^+\widehat{\rho} - \widehat{\rho}\widehat{\sigma}^-\widehat{\sigma}^+\right]. \tag{21}$$

which pushes the population towards the excited state.

Effective incoherent pumping rate. Emission by the emitters into the cavity occurs via the light-matter coupling term in (20). If the pump rate $\Gamma_{\rm P}$ well exceeds the Rabi frequency Ω_R, the dynamics of the emitter can be adiabatically eliminated and the coherent Rabi oscillations typical of the Jaynes–Cummings model of cavity-QED [51,57] are replaced by an irreversible emission into the cavity mode.

If we further assume that the in-cavity field is weak enough not to affect the population inversion, gain saturation is not significant and we obtain an effective incoherent pumping of the form (19) with a rate

$$\gamma^{\rm eff,0}_{\rm pump} = \frac{4\Omega_R^2}{\Gamma_{\rm P}}. \tag{22}$$

Of course, such a rate is only obtained when the emitter is exactly on resonance with the photon mode, otherwise the pumping rate is reduced according to a Lorentzian lineshape of width $\Gamma_{\rm P}$ around the resonant point $\omega = \omega_{\rm em}$,

$$\gamma^{\rm eff}_{\rm pump}(\omega) = \gamma^{\rm eff,0}_{\rm pump} \, \frac{\Gamma_{\rm P}^2/4}{(\omega-\omega_{\rm em})^2+\Gamma_{\rm P}^2/4}. \tag{23}$$

Including this ω dependence is straightforwardly done in a linear system: for each mode at frequency $\overline{\omega}$, one can write an incoherent pumping term of the form (19) with an effective $\gamma^{\rm eff}_{\rm pump}(\omega)$ evaluated at the mode frequency $\omega = \overline{\omega}$.

Things get more complex in interacting many-mode models, where different frequencies ω have to be considered for the different transitions between many-body eigenstates. At a simplest level of approximation [58], the standard Lindblad term (19) can be replaced by a generalized term in the form [59]

$$\mathscr{L}_{\rm em}(\rho) = \frac{\gamma^{\rm eff,0}_{\rm pump}}{2} \sum_j \big[\widetilde{a}^\dagger_i \rho \widehat{a}_i + \widehat{a}^\dagger_i \rho \widetilde{a}_i - \widehat{a}_i \widetilde{a}^\dagger_i \rho - \rho \widetilde{a}_i \widehat{a}^\dagger_i \big], \tag{24}$$

where the sum runs over the lattice sites j and the frequency dependence of the pumping process is encoded by the modified jump operator $\widetilde{a}^\dagger_j$ such that

$$\langle f' | \widetilde{a}^\dagger_j | f \rangle = \frac{\Gamma_{\rm P}/2}{i(\omega_{f,f'}-\omega_{\rm em})+\Gamma_{\rm P}/2} \langle f' | \widehat{a}^\dagger_j | f \rangle \tag{25}$$

for each pair of many-body states f, f' with respectively N and $N+1$ photons. Physically, this means that the effective jump amplitude from the many-body state f with N photons to the many-body state f' with $N+1$ photons under the creation of a photon in the j cavity mode depends on the frequency difference $\omega_{f,f'} = \omega_{f'} - \omega_f$ of the many-body states.

Inserting the explicit expression (25) into the Lindblad term (24) leads to a Lorentzian dependence of the $f \to f'$ transition rate on the frequency difference $\omega_{f,f'}$,

$$\mathscr{T}_{\rm pump}(f \to f') = \gamma^{\rm eff}_{\rm pump}(\omega_{f,f'}) \sum_j \big| \langle f' | \widehat{a}^\dagger_j | f \rangle \big|^2, \tag{26}$$

to be compared with the frequency-independent transition rate due to the loss processes discussed in Section 2.2.1,

$$\mathscr{T}_{\rm loss}(f' \to f) = \gamma_{\rm loss} \sum_j \big| \langle f | \widehat{a}_j | f' \rangle \big|^2. \tag{27}$$

On top of this, the imaginary part of the resonance factor in (25) leads, upon substitution into the Lindblad term (24), to an additional conservative Hamiltonian term giving a (typically small) energy shift of the energy levels of the photonic system, which can be physically understood as a consequence of the effective refractive index of the population-inverted emitters. In the simplest case of a linear single-mode cavity, an explicit calculation leads to a frequency-shift of the cavity mode by

$$\delta\omega_0 = \frac{\Gamma_P \gamma^{\rm eff,0}_{\rm pump}/4}{(\omega_{\rm em}-\omega_0)^2+\Gamma_P^2/4} \, (\omega_{\rm em}-\omega_0); \tag{28}$$

note how this effect has an opposite sign compared to the usual refractive index of ground-state atoms so, in contrast to the usual polariton splitting [5], it leads to the attraction of the cavity mode towards the emitter in a sort of *frequency pulling* effect.

It is important to note that the generalized master equation (24) is only valid under a sort of perturbative expansion in the strength of the driving/dissipation processes: the jump amplitudes in (25) are in fact evaluated in terms of the energies of the conservative eigenstates. Writing master equations that go beyond this approximation and allow to deal with stronger driving/dissipation regimes is a topic of present-day research [58,60,61].

Gain saturation. As mentioned above, the effective description based on (24) also assumes that the emission into the photon mode is weak enough not to deplete the population inversion in the emitters. Of course, bosonic stimulation of the emission processes makes this constraint more severe when there is a sizable population in the photonic modes, $\gamma_{\rm pump}^{\rm eff}\, n_{\rm ph} \ll \Gamma_{\rm P}$.

In order to go beyond this assumption and account for those gain-saturation effects that play a major role in many physical phenomena, one needs to fully include the back-reaction effect of the emission onto the emitter dynamics. At the quantum level, this requires a complete description of the emitter and field dynamics: this is a challenging many-body task and typically has to be carried out under some other simplifying hypothesis, e.g. mimicking gain saturation by means of two-photon loss processes or performing some Gutzwiller site-decoupling approximation [62]. At the semiclassical level, instead, calculations can be performed in terms of generalized mean-field equations inspired by the semiclassical theory of lasers as we are going to see in the next section.

Alternative configurations. To conclude this section, it is important to also mention that different configurations to obtain a frequency-dependent pumping were proposed in [63] using parametric emission processes. The key element of such schemes is to replace the two-level emitter used in (20) with an additional ancilla cavity displaying strong losses $\Gamma_{\rm anc}$ described by a standard Lindblad master equation. Parametric processes then generate pairs of photons in the photonic mode and in the ancilla cavity according to

$$H = \hbar\omega_0 \widehat{a}^\dagger \widehat{a} + \hbar\omega_{\rm anc}\, \widehat{b}^\dagger \widehat{b} + \left[\hbar\Omega_{\rm par} e^{-i\omega_{\rm par} t}\, \widehat{a}^\dagger \widehat{b}^\dagger + \hbar\Omega_{\rm par}^* e^{i\omega_{\rm par} t}\, \widehat{a}\widehat{b}\right]; \tag{29}$$

an effective irreversibility naturally arises if the ancilla decay rate $\Gamma_{\rm anc}$ well exceeds the parametric emission rate $\Omega_{\rm par}$. Right at the parametric resonance point, this gives an effective pumping rate,

$$\gamma_{\rm pump}^{\rm eff,0} = \frac{4|\Omega_{\rm par}|^2}{\Gamma_{\rm anc}}. \tag{30}$$

Such a value, together with the parametric resonance condition $\omega_{\rm par} - \omega_{\rm anc} = \omega_0$ can be directly inserted in the theory of equation (24) and leads to closely analogous results up to the many-body level. Such a strategy was experimentally put into practice in [64] to generate a Mott insulator state of impenetrable photons.

Alternative photon-number-conserving schemes to force microwave photons to scatter from high- to low-momentum states and eventually accumulate into a condensate were proposed in [65]. Interesting connections between nonequilibrium condensation and quantum transport and non-Hermitian topology were then highlighted in [66]. The subtle interplay of dissipative stabilization techniques with Floquet engineering was investigated in [67] with the goal of stabilizing interesting states of a strongly interacting Bose gas in the presence of a synthetic magnetic field. More generally, note how related techniques for autonomous dissipative stabilization of desired quantum states are of widespread use beyond quantum fluids of light for various tasks in quantum science and technology [68–72].

3. Weakly interacting fluid

The new possibilities opened for quantum fluids of light by the presence of the driving and dissipation processes were first addressed in the context of weakly interacting fluids for which a mean-field approximation is legitimate. Such regimes have been long studied in the context of nonlinear optics and laser physics and, more recently, in the context of polariton fluids and polariton condensates. The literature on this physics is immense and we refer the interested reader to recent review articles [5,73]. With no hope of completeness, in what follows we will focus on a few cases where the physics is—to our eyes—most clear and illustrative of the general principles.

3.1. *Mean-field approximation*

The key idea of the mean-field approximation is to write an approximate equation of motion for the expectation value of the field operator $\psi(\mathbf{r}_\parallel, t) = \langle \widehat{\Psi}(\mathbf{r}_\parallel, t) \rangle$. Such an equation of motion can be derived by taking the Heisenberg equation for the field operator and then factorizing all operator products. Usually, this factorization assumption is accurate as long as the fluctuations around the mean-field are small, which is generally the case if interactions between the particles are weak.

Application of this procedure to the conservative Hamiltonian (15) leads to the Heisenberg equation

$$i\hbar \frac{\mathrm{d}\widehat{\Psi}(\mathbf{r}_\parallel, t)}{\mathrm{d}t} = [\widehat{\Psi}, H] = \hbar\omega_o \widehat{\Psi}(\mathbf{r}_\parallel) - \frac{\hbar^2}{2m}\nabla_\parallel^2 \widehat{\Psi}(\mathbf{r}_\parallel) + \hbar V(\mathbf{r}_\parallel)\,\widehat{\Psi}(\mathbf{r}_\parallel) + \hbar g_{\mathrm{nl}} \widehat{\Psi}^\dagger(\mathbf{r}_\parallel)\,\widehat{\Psi}(\mathbf{r}_\parallel)\,\widehat{\Psi}(\mathbf{r}_\parallel), \tag{31}$$

on which the factorization approximation

$$\langle \widehat{\Psi}^\dagger(\mathbf{r}_\parallel)\,\widehat{\Psi}(\mathbf{r}_\parallel)\,\widehat{\Psi}(\mathbf{r}_\parallel) \rangle \approx \left|\psi(\mathbf{r}_\parallel, t)\right|^2 \psi(\mathbf{r}_\parallel, t) \tag{32}$$

gives the usual Gross–Pitaevskii equation for an interacting Bose–Einstein condensate,

$$i\frac{\partial \psi}{\partial t} = \left[\omega_o - \frac{\hbar\nabla^2}{2m^*}\right]\psi + V\psi + g_{\mathrm{nl}}|\psi|^2\psi. \tag{33}$$

Necessary conditions for the validity of this mean-field approach can be obtained from the general many-body theory of dilute Bose–Einstein condensates at equilibrium [1,74]. For instance, for three-dimensional gases, the condition can be expressed in terms of a diluteness condition $n_{3d}\, a_{\mathrm{sc}}^3 \ll 1$, where n_{3d} is the three-dimensional density and a_{sc} is the atom-atom collisional scattering length, related to the interaction parameter by $g_{\mathrm{nl}} = 4\pi\hbar^2 a_{\mathrm{sc}}/m$. More subtle conditions have to be imposed in low-dimensional geometries, but a quite general formulation involves the characteristic kinetic and interaction energies, $\varepsilon_{\mathrm{kin}} = \hbar^2 n^{2/d}/2m \gg \varepsilon_{\mathrm{int}} = g_{\mathrm{nl}} n$ or, equivalently, the number of particles per healing length, $n\xi^d \gg 1$ where n is the d-dimensional density and $\xi = \sqrt{\hbar^2/m g_{\mathrm{nl}} n}$ is the healing length characterizing the microscopic structure of the weakly interacting fluid.

The same factorization procedure can be performed on the pumping and loss terms introduced in Section 2.2. The coherent pump is straightforwardly included at the level of the Heisenberg equation. As the corresponding Hamiltonian term (18) is linear in $\widehat{\Psi}$, no additional factorization approximation has to be made. As a result, one obtains a forcing term in the equation of motion for ψ of the form:

$$\ldots + \eta\,\mathscr{E}(\mathbf{r}_\parallel, t). \tag{34}$$

The linear loss and incoherent pumping terms (17) and (19) give linear, phase-insensitive gain and loss terms of the form

$$\ldots - \frac{\gamma_{\mathrm{loss}}}{2}\psi + \frac{\gamma_{\mathrm{pump}}}{2}\psi, \tag{35}$$

from which it is immediate to see how an unlimited exponential growth may arise if $\gamma_{\mathrm{pump}} > \gamma_{\mathrm{loss}}$ and no gain saturation mechanism is included in the model.

3.1.1. *Gain saturation & frequency selectivity*

Gain saturation can be included starting from the model of Section 2.2.4. In analogy to the semiclassical equations of lasers [56,57], we have to write the equations of motions for the single-mode field amplitude $\alpha = \langle \widehat{a} \rangle$,

$$\frac{\mathrm{d}\alpha}{\mathrm{d}t} = -i\omega_0\alpha - i\Omega_R\sigma^- - \frac{\gamma_{\mathrm{loss}}}{2}\alpha, \tag{36}$$

as well as for the expectation values of the emitter operators $\sigma^{\pm,z} = \langle \hat{\sigma}^{\pm,z} \rangle$. Performing all the factorization approximations of mean-field theory, we obtain

$$\frac{\mathrm{d}\sigma^z}{\mathrm{d}t} = \Gamma_\mathrm{P}(1-\sigma^z) - 2i\Omega_R(\sigma^+\alpha - \sigma^-\alpha^*), \tag{37}$$

$$\frac{\mathrm{d}\sigma^-}{\mathrm{d}t} = -i\omega_\mathrm{em}\sigma^- - \frac{\Gamma_\mathrm{P}}{2}\sigma^- + i\Omega_R\sigma^z a. \tag{38}$$

These equations for the single-mode configuration can be straightforwardly extended to spatially continuous geometries with many uniformly distributed emitters of in-plane density n_em. For this, we introduce space-dependent emitter spin variables $\sigma^{\pm,z}(\mathbf{r}_\parallel)$ and we replace the localized field amplitude α with the continuous field $\psi(\mathbf{r}_\parallel)$.

In the so-called good-cavity limit where the emitter pump rate Γ_P is much faster than the field dynamics and of the light-matter coupling Ω_R, one can eliminate the emitter degrees of freedom and write an effective equation of motion for the field only,

$$i\frac{\partial\psi}{\partial t} = \left[\omega_o - \frac{\hbar\nabla^2}{2m^*}\right]\psi + V\psi + g_\mathrm{nl}|\psi|^2\psi + \frac{i}{2}\left[\frac{P - 2i\,\delta\omega_0}{1+|\psi|^2/n_s} - \gamma_\mathrm{loss}\right]\psi + \eta\,E_\mathrm{inc}(\mathbf{r},t) \tag{39}$$

where the cavity mode experiences an effective pumping

$$P = \frac{n_\mathrm{em}\,\Omega_R^2\Gamma_P}{(\omega_\mathrm{em}-\omega_0)^2 + \Gamma_P^2/4} \tag{40}$$

with a saturation density

$$n_s = \frac{(\omega_\mathrm{em}-\omega_0)^2 + \Gamma_P^2/4}{2\Omega_R^2} \tag{41}$$

and a Lorentzian frequency-dependence of linewidth Γ_P analogous to the one of (26). In analogy to what was found in (42), the presence of the emitters also leads to a frequency-pulling effect towards the emitter of magnitude

$$\delta\omega_0 = \frac{n_\mathrm{em}\,\Omega_R^2}{(\omega_\mathrm{em}-\omega_0)^2 + \Gamma_P^2/4}\,(\omega_\mathrm{em}-\omega_0). \tag{42}$$

The formulas starting (39)–(42) implicitly assume that the cavity field dynamics takes place in a very narrow frequency band around ω_0. At a slightly more sophisticated level, we can Taylor-expand the frequency-dependence of the different quantities around ω_0. For instance, the frequency-dependence of the pumping rate P can be effectively modeled [75] by replacing

$$P \to P\left[1 - \frac{2(\omega_0-\omega_\mathrm{em})}{(\omega_\mathrm{em}-\omega_0)^2+\Gamma_P^2/4}\left(i\frac{\partial}{\partial t} - \omega_0\right)\right] \tag{43}$$

and letting the last time-derivative to only act on the field ψ. In some physical models of lasing, such a frequency-dependence of gain is crucial to theoretically recover a stable laser operation at the bottom of the photon band as observed in the experiment.

As a final point, it is important to highlight that equations analogous to (39) have been derived in several other contexts from different points of view. The approach of this article is inspired from the many-body theory of dilute Bose gases: in this framework, it is then natural to call this equation *generalized nonequilibrium Gross–Pitaevskii equation*. The very similar equations that are considered in the context of nonlinear dynamics typically go under the name of complex Ginzburg–Landau equations [76,77]. In the nonlinear optics literature, they go under the name of *Lugiato–Lefever equation*: originally formulated in [78], this equation is still now a powerful workhorse for the description of optical devices based on Kerr cavity solitons and frequency combs [73].

3.1.2. *Quantum fluctuations beyond mean-field*

Within a semiclassical approach, effects beyond the mean-field can be described within the so-called truncated Wigner approximation [55,79] by adding a stochastic white noise term $\xi(\mathbf{r}_\parallel, t)$ on the right-hand side of the motion equation (39) so as to account, at least at a lowest order, for quantum fluctuations. In the case of coherent pumping, the complex-valued noise term must have a random phase and its variance is to be set to

$$\left\langle \xi^*(\mathbf{r}_\parallel, t)\, \xi(\mathbf{r}'_\parallel, t') \right\rangle = \frac{\gamma_{\rm loss}}{2}\, \delta^{(2)}(\mathbf{r}_\parallel - \mathbf{r}'_\parallel)\, \delta(t-t'); \tag{44}$$

this is the minimum noise level as determined by the quantum fluctuations associated to the discreteness of the photon in the loss process. Of course, a higher noise level is found in incoherent pumping configurations [80] where additional fluctuations are given by spontaneous events in the pumping process,

$$\left\langle \xi^*(\mathbf{r}_\parallel, t)\, \xi(\mathbf{r}'_\parallel, t') \right\rangle = \frac{1}{2}\left(\gamma_{\rm loss} + \frac{\gamma_{\rm pump}}{1+|\psi|^2/n_S}\right) \delta^{(2)}(\mathbf{r}_\parallel - \mathbf{r}'_\parallel)\, \delta(t-t'). \tag{45}$$

Further sources of quantum noise may stem from the interaction of the Bogoliubov modes of the photon fluid with phonon modes in the solid-state crystal hosting the fluid of light [81]. Generalization of truncated Wigner methods to systems involving emitters as described e.g. in the Hamiltonian model of (20) are under way [82].

As typical of Wigner representations [55], for any product of fields $\psi(\mathbf{r}_\parallel)$ and $\psi^*(\mathbf{r}'_\parallel)$, the statistical average over the noise provides information on the corresponding *symmetrized* product of quantum operators $\widehat{\Psi}(\mathbf{r}_\parallel)$ and $\widehat{\Psi}^\dagger(\mathbf{r}'_\parallel)$, so commutators have to be subtracted to obtain the more standard normal-ordered quantities. While this is a quite trivial step for single-time operator products, it poses serious challenges for calculation multi-time quantities [83].

Interestingly, the driven-dissipative condition makes the truncated Wigner approach much more stable than in the conservative case, as the field fluctuations get to a driven-dissipative steady-state determined by the interplay of stochastic noise and dissipation well before approaching an inaccurate classical field thermal equilibrium state [84]. While this is often sufficient to get physically reliable predictions for the field correlation functions [79], it is important to note that the approximation of truncating higher-order noise terms [85] that underlies (45) typically loses accuracy when strong interactions and/or very non-perturbative processes in the quantum fluctuations are considered, such as quantum tunneling in bistable systems [86,87]. Quantitative studies of the limitations of the truncated Wigner approach [88] and of possible avenues to include the higher-order derivative terms [89] are the topic of current research.

3.2. *Coherent pumping*

The configuration where the new possibilities opened by driving and dissipations are clearest is the coherent pumping one. This configuration was exploited in the first experiments demonstrating superfluid light, as the flow speed and the density of the fluid can be directly controlled by the incidence angle (i.e. the in-plane wavevector), the frequency and the intensity of the incident field [90,91]. As a key difference from equilibrium condensates, the oscillation frequency of the field is not bound to the chemical potential but is freely determined by the one of the incident coherent field. As a result, the equation of state becomes richer and new phenomena can be observed.

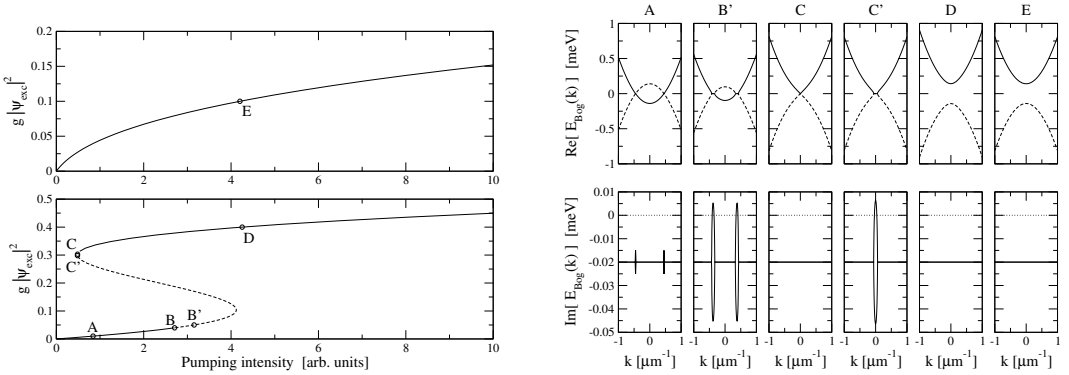

Figure 2. Left panels: plot of the equation of state of the fluid of light, expressed as fluid density as a function of pump intensity for two different incident frequencies in respectively the optical limiter regime (top) and the bistable regime (bottom). The dashed line indicates the dynamically unstable regions. Right panel: real part (top) and imaginary part (bottom) of the excitation frequencies for the nonequilibrium Bogoliubov modes corresponding to the points indicated as A, B', C, C', D, E in the left panel.

3.2.1. *Homogeneous fluid*

In the simplest case of a monochromatic incident field at $\omega_{\rm inc}$ with a spatially homogeneous profile, the fluid is at rest and the equation of state

$$\left[\left(\omega_0 + g_{\rm nl}|\psi|^2 - \omega_{\rm inc}\right)^2 + \frac{\gamma_{\rm loss}^2}{4}\right]|\psi|^2 = |\eta\, E_{\rm inc}|^2, \tag{46}$$

gives a complex nonlinear dependence of the density $|\psi|^2$ on the different parameters of the incident field. Some of the peculiar features of these nonequilibrium fluids are visually illustrated in Figure 2: the prediction of the equation of state (46) is displayed in the two left panels for the two cases of a pump frequency respectively below $\omega_{\rm inc} < \omega_0$ (top) and above $\omega_{\rm inc} > \omega_0$ (bottom) the bare resonance frequency (we are assuming $g_{\rm nl} > 0$): in the former case, the in-cavity intensity (proxied by $g|\psi_{\rm exc}|^2$ in the figure) grows monotonically but sublinearly with the pump intensity $|E_{\rm inc}|^2$; in the latter case, bistability effects are apparent, with two values of the density $|\psi|^2$ being available for the same value of the pump intensity $|E_{\rm inc}|^2$ (the intermediate branch is dynamically unstable).

Further consequences of the nonequilibrium condition are visible in the right panels, where the dispersion of the Bogoliubov modes on top of the homogeneous fluid [5,90] are plotted for the different operating points indicated by the capital letters in the left panels. As the oscillation frequency of the field ψ is not bound to $\omega_0 + g_{\rm nl}|\psi|^2$ as in the equilibrium case but is freely tunable via the incident frequency $\omega_{\rm inc}$, a wider range of behaviours can be observed depending on the pumping conditions. In particular, the Bogoliubov modes display a sonic long-wavelength behaviour $\omega = c_s|\mathbf{k}|$ only for a very specific operating point (C) at the end of the upper branch of the bistability loop. Away from this point, the dispersion may display finite gaps (D, E) and, even, precursors (A) or fully fledged (B, C') dynamical instabilities. Detailed experimental studies of the Bogoliubov dispersion in the different pumping regimes have been carried out by pump-probe spectroscopy in [92].

Going beyond mean-field, the consequences of the driven-dissipative condition are also visible in the steady-state fluctuations of the field ψ, which are well larger than the zero-point fluctuations of the Bogoliubov ground state of the corresponding equilibrium system. Within

a Bogoliubov picture, the loss process for a particle at momentum $\mathbf{k}$ involves in fact either the destruction of a quasi-particle at $\mathbf{k}$ or the creation of a quasi-particle at $-\mathbf{k}$. The overall magnitude of these fluctuations roughly corresponds to a temperature of the order of the interaction energy $g_{\rm nl}|\psi|^2$ and also display interesting correlation properties [93].

3.2.2. *Acoustic horizons and analog Hawking radiation*

This tunability of the Bogoliubov modes can be exploited to observe exciting new behaviours in spatially inhomogeneous configurations when the spatial profile of the coherent pump is suitably structured. In this perspective, a variety of configurations have been investigated in the literature, for instance vortices and vortex lattices that appear under a coherent pump carrying orbital angular momentum [94].

As a specific most exciting example, we focus here on configurations featuring a sonic horizon separating an upstream region of sub-sonic flow $c_u > v_u$ from a downstream region of super-sonic flow $v_d > c_d$ where $c_{u,d}$ and $v_{u,d}$ are respectively the sound and flow speeds in the two u,d regions. From the point of view of sound propagation, this configuration displays strong analogies with light propagation in the neighborhood of a black hole in gravitational physics and, upon quantization, sonic analogs of Hawking radiation have been anticipated to be emitted by the acoustic horizon [95].

With a careful design of the coherent pump, such analog black holes naturally arise as the driven-dissipative steady-state of a photon fluid. A natural possibility to achieve this [96] is to use a monochromatic pump and to design its phase profile so as to have a small in-plane wavevector in the upstream region and a larger one in the downstream region. Alternatively, the downstream region can be left unpumped so that the photon fluid is able to ballistically expand into this region. This latter configuration was experimentally realized in [97]. A spatially-resolved experimental characterization of the Bogoliubov modes on the two sides of the horizon has been performed in [98], explicitly showing the transition from a sub- to a super-sonic flow as the horizon is crossed: in the experiment, a super-sonic flow is signalled by the positive-norm branch of the Bogoliubov dispersion being pushed down to negative frequencies.

The on-going challenge is then to obtain experimental evidence of the analog Hawking emission by the acoustic horizon: to this purpose, numerical studies based on the Wigner formalism have shown that a clear signature of the Hawking radiation is present in the correlation function of density fluctuations on opposite sides of the horizon [96,97]. Physically, this correlation feature reflects the correlations between the Hawking phonon emitted outside the horizon into the sub-sonic region and its partner that propagates inside the horizon into the super-sonic region. Most interestingly, in contrast to atomic fluids where destructive measurements of atomic density profile are typically needed [99], intensity fluctuations are a quantity of direct and real-time experimental access in driven-dissipative photon fluids: radiative losses directly transfer the correlation functions of the in-cavity field into the ones of the emitted light, where the Hawking signal can be observed as peculiar intensity correlations of the emitted light.

Note that the extra fluctuations induced by the driven-dissipative nature [93] lead to a stimulation of the Hawking processes and, then, a reinforcement of the overall magnitude of the correlation signal. While this makes the correlations easier to detect, the resulting stimulated rather than spontaneous nature of the process may wash out the peculiar quantum entanglement features of Hawking radiation predicted in [100] in the context of analog models based on atomic condensates.

3.2.3. *Integer quantum Hall effect*

One of the most intriguing family of phenomena of quantum condensed matter physics is the quantum Hall effect [101]. This effect was originally discovered in two-dimensional electron

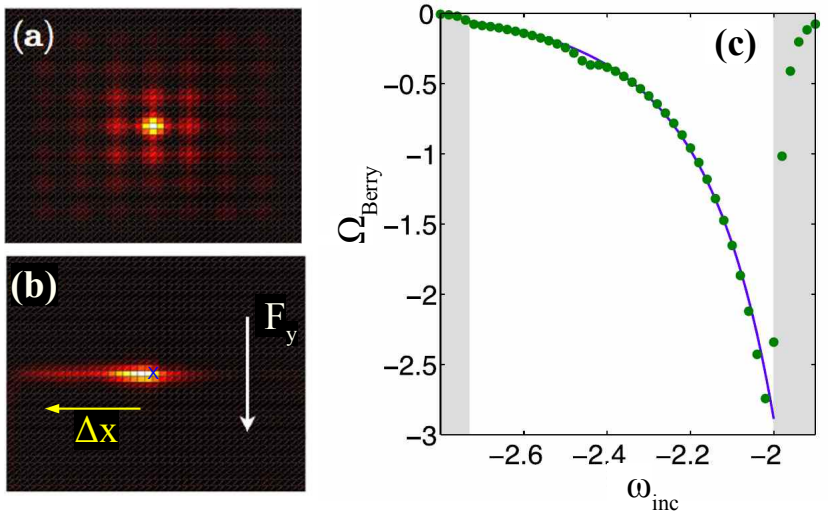

Figure 3. Left (a)–(b) panels: color plots of the numerically calculated steady-state intensity distribution in a coherently pumped $q = 5$ photonic Harper–Hofstadter model. The pump is localized on the central site and is resonant with the lowest photonic band. The loss rate is taken to be larger than the bandwidth $\gamma_{\rm loss}/\Delta\omega_{\rm band} = 2$, so as to be in the integer quantum Hall (IQH) regime. In the upper (a) panel, no external force is present and the distribution has a $\pi/2$ rotational symmetry. In the lower (b) panel, a force along the negative y direction is applied, so the intensity distribution moves leftwards along the transverse x direction. The magnitude of this displacement agrees with the prediction of the driven-dissipative IQH formula (48). Right panel: for a loss rate smaller than the bandwidth $\gamma_{\rm loss}/\Delta\omega_{\rm band} \simeq 1/30$ of the lowest band of a $q = 3$ Harper–Hofstadter, we are in the anomalous quantum Hall regime and the displacement is determined by the average of the Berry curvature over all states resonant with the pump frequency $\omega_{\rm inc}$. Within a photonic band (white region), the value of the Berry curvature extracted from the numerically calculated transverse shift (green points) are in good agreement with the value of the Berry curvature extracted from the Harper–Hofstadter band structure. Panels adapted from [102].

gases subject to strong magnetic fields and cooled to ultralow temperatures. While in room-temperature metals the transverse Hall resistivity ρ_{xy} shows a structureless linear dependence on the applied magnetic field B, the *quantum* Hall effect is visible as a series of plateaux in ρ_{xy} when the so-called filling factor

$$\nu = \frac{2\pi\hbar n_{2D}}{eB} \tag{47}$$

is in the neighborhood of integer (the so-called *integer quantum Hall (IQH)* effect) or fractional (*fractional quantum Hall (FQH)* effect) values. In this section, we are going to focus on the IQH effect, while a brief discussion of the FQH in an optical context will be given later on in Section 4.

Physically, the origin of the IQH can be traced to the complete and homogeneous filling of all states in the ν lowest Landau levels in the magnetic field B. In electronic systems where the number of electrons is conserved, the value of ν can be fixed by tuning the externally applied magnetic field B or the electronic density n_{2D} with suitable gates, so as to fix the Fermi energy between two Landau levels. While this simple argument explains the quantized value of the conductivity, the finite width of the plateaux results instead from a more subtle interplay

between localized and delocalized electronic states in the unavoidable disorder of any realistic system [101].

In analogy to these advances in quantum condensed matter systems, a strong interest is being devoted to the so-called topological photonic systems where new phenomena stemming from the non-trivial band topology of the photonic states have been observed, e.g. unidirectionally propagating chiral edge states [103]. In this context, a basic ingredient is the so-called synthetic magnetic field acting on photons: in the presence of a strong and uniform synthetic magnetic field, photonic modes closely resemble Landau levels and skipping orbits appear on the edges.

Even though in driven-dissipative photonic systems particles are continuously lost and replenished and no Fermi–Dirac statistics is available to impose a uniform population, a recent work [102] has pointed out that a spatially very localized coherent pump can be used to uniformly drive all states within a given Landau level. Even though the occupation is not pinned to 1 as it happens in the electronic case, the uniformity of the population is sufficient to observe a quantized response under the effect of a uniform force. In our photonic case, such a force—a sort of synthetic electric field—is obtained with a uniform spatial gradient of the cavity resonance frequency as described by a linearly varying potential term $V(\mathbf{r}_\parallel) = -\mathbf{F}\cdot\mathbf{r}_\parallel$ in (39).

Focusing for concreteness on the square-lattice Harper–Hofstadter model at $1/q$ flux per plaquette with a large q, the lateral spatial shift of the center of mass of the photon intensity distribution was in fact predicted [102] to be

$$\Delta x = \frac{q\mathscr{C}F}{\pi\gamma_{\rm loss}} \tag{48}$$

where a force of magnitude F is applied along the direction y and $\mathscr{C} = 1$ is the Chern number of the photonic band under examination: the driven-dissipative nature results in the transverse susceptibility being proportional to the lifetime $\gamma_{\rm loss}^{-1}$ times a quantized value.

While Landau levels in continuous space are perfectly flat in energy, the energy bands of discrete topological models on a lattice (e.g. the Harper–Hofstadter or the Haldane models) may display a significant bandwidth $\Delta\omega_{\rm band}$ in energy. In our driven-dissipative systems, this offers a further knob to stabilize and manipulate different states of the quantum fluid: depending on the relative value of the energy bandwidth $\Delta\omega_{\rm band}$ and of the loss rate $\gamma_{\rm loss}$, one can in fact transition from a IQH regime where $\gamma_{\rm loss} \gg \Delta\omega_{\rm band}$ and the coherent pumping uniformly drives all states within the band, to an anomalous Hall regime where $\gamma_{\rm loss} < \Delta\omega_{\rm band}$ and the frequency of the coherent drive specifically selects a set of resonant states. In this latter case, the lateral shift is no longer quantized and is determined by the averaged value of the Berry curvature over the set of resonant states. This provides a further example where the driven-dissipative nature of the photon fluid can be exploited to stabilize interesting many-body states and probe their physical properties.

An experiment that exploits driving and dissipation for a comprehensive study of anomalous and integer quantum Hall effect in a photonic Haldane model using a frequency-encoded synthetic dimension platform based on an optical fiber loop was recently reported in [104].

3.3. *Incoherent pumping*

In the previous subsection we have discussed coherent pumping schemes, where the phase of the in-cavity field is locked to the one of the incident field. A different range of physical phenomena are observed when an incoherent pump is used to inject photons in the system in a phase-insensitive way: as a most significant example, we will focus on the spontaneous generation of coherence via a nonequilibrium phase transition, a phenomenon that opens the way towards the study of critical phenomena in a novel nonequilibrium setting. While the

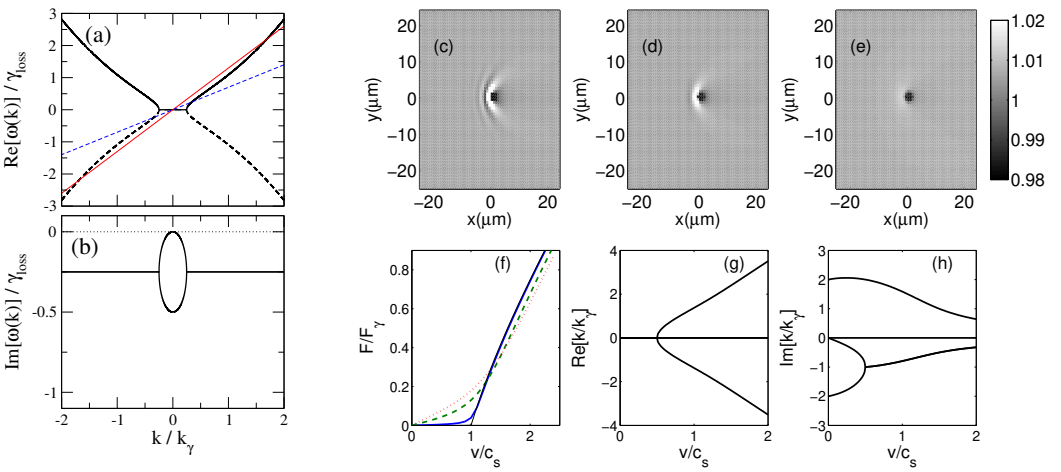

Figure 4. Left panels: plot of the real (a) and imaginary (b) parts of the dispersion of the collective excitations of a nonequilibrium condensate under incoherent pumping at $P/\gamma_{\rm loss} = 2$ with $\gamma_{\rm loss}/g_{\rm nl}|\psi|^2 = 1$. For small k values, the dispersion displays a diffusive plateau with a zero real part and a quadratically growing imaginary part. The oblique straight lines correspond to the Landau–Cherenkov $\omega = kv$ condition for a particle moving at $v/c_s = 0.7$ (blue dashed) or $v/c_s = 1.3$ (red solid). Wavevector is measured in units of k_γ such that $\hbar k_\gamma^2/2m = \gamma_{\rm loss}$. Right (c)–(h) panels: generalized Landau criterion for nonequilibrium condensates. Panels (c)–(e) show the density perturbation induced in a fluid moving in the positive x direction by an impurity at rest. The different panels refer to different values of the condensate velocity $v/c_s = 1.5$, 1, 0.4 across the (equilibrium) speed of sound $c_s = \sqrt{g_{\rm nl}|\psi|^2/m}$. Panel (f) shows the (normalized) force exerted by the fluid on the defect as a function of the condensate velocity v/c_s for different values of the nonequilibrium parameter $\gamma_{\rm loss}/g_{\rm nl}|\psi|^2 = 0$, 0.1, 1, 2. For the smallest $\gamma_{\rm loss}$ values, the sudden onset of friction that is visible in the vicinity of the critical speed $v/c_s = 1$ is a nonequilibrium counterpart of the Landau critical velocity of equilibrium superfluids [1,105]. Panels (g)–(h) show a cut of the real and the imaginary part of the wavevector of the collective excitations emitted in the negative x direction as a function of the speed for an intermediate loss case with $\gamma_{\rm loss}/g_{\rm nl}|\psi|^2 = 1$. The sudden onset of friction in (f) corresponds to the singular point that is visible in (g)–(h) slightly below $v/c_s = 1$. Panels (c)–(h) are adapted from [75].

underlying physics is very similar in the different systems, this phenomenon takes distinct names in distinct communities, e.g. laser oscillation in the optical literature or nonequilibrium Bose–Einstein condensation in the polaritonic one. An interdisciplinary review of this physics can be found in [8].

3.3.1. *Mean-field effects*

Restricting again to a weak interaction regime, a theoretical description of the field dynamics can be obtained at the mean-field level starting from the generalized Gross–Pitaevskii equation (39). In the absence of any coherent incident field $E_{\rm inc} = 0$, the system displays a marked threshold at $P_c = \gamma_{\rm loss}$ between a trivial $\psi = 0$ steady-state solution for a weak pump $P < \gamma_{\rm loss}$ to a condensed (or lasing) solution for a strong pump $P > \gamma_{\rm loss}$. In this latter regime, the steady-state

intensity is stabilized by nonlinear gain saturation effects to

$$|\psi|^2 = n_s\left(\frac{P}{\gamma_{\rm loss}} - 1\right) \tag{49}$$

but the phase of ψ remains free and is randomly chosen at every instance of the experiment. Under the $E_{\rm inc} = 0$ condition, the equation of motion (39) displays in fact a global $U(1)$ symmetry $\psi \to \psi\, e^{i\varphi}$ for arbitrary φ and this symmetry is spontaneously broken above threshold where the field ψ selects a specific and uniform phase across the whole system and its time-evolution displays a monochromatic oscillation at the intensity-dependent frequency $\omega = \omega_0 + g|\psi|^2$. The combination of a monochromatic oscillation in time and of a spatially uniform phase showcases the interest of this configuration as a source of spatio-temporally coherent light.

Diffusive Goldstone mode. Even though the driven-dissipative steady-state shares many properties with a standard Bose–Einstein condensate at equilibrium, one must not forget that the nonequilibrium condition is responsible for important deviations in the collective properties of the fluid, in particular for what concerns the Goldstone mode that is associated to the spontaneously broken $U(1)$ symmetry. As it is illustrated in Figure 4(a)–(b), the dispersion of the long-wavelength, low-frequency collective excitations does not show the usual sonic behaviour $\omega = c_s|\mathbf{k}|$ of equilibrium condensates with a speed of sound c_s, but rather displays a diffusive plateau in the form $\omega = -i\alpha k^2$ with a real and positive α. The usual behaviour with propagating collective excitations is only recovered at shorter wavelengths. The transition between the two regimes is typically associated to an exceptional point in the dispersion, whose position is determined by the strength of the departure from equilibrium, namely by the value of the loss rates: the larger $\gamma_{\rm loss}$, the wider the diffusive plateau. The theoretical prediction of a diffusive behaviour of the Goldstone mode of a nonequilibrium condensate has been recently confirmed in a pump-and-probe experimental measurement of the dispersion of the collective modes of an exciton-polariton condensate [106].

Generalized Landau criterion for superfluidity. This diffusive behaviour has been anticipated in [75] to impact the conceptual meaning of the Landau criterion for superfluidity in the driven-dissipative context. In stark contrast to the equilibrium case, it is shown in Figure 4(a) how the real part of the dispersion has an intersection with the Landau–Cherenkov $\omega = k\,v$ straight line for any non-zero value of v. A naive application of the Landau criterion for superfluidity [1,105] would then predict that an impurity moving across a fluid will experience a significant friction force for any value of the flow speed v, with no specific feature at the (equilibrium) speed of sound $c_s = \sqrt{g_{\rm nl}|\psi|^2/m}$.

This prediction is shown in Figure 4(f) to disagree with a full numerical solution of the generalized Gross–Pitaevskii equation (39): for small or moderate values of the nonequilibrium parameter $\gamma_{\rm loss}/g_{\rm nl}|\psi|^2$, the friction force exerted by an impurity at rest onto a moving fluid displays in fact a sudden upwards kink at a value of v/c_s close to the (equilibrium) critical velocity $v_{\rm cr} = c_s$. Such a change in behaviour can be associated to the singularity in the wavevector of the collective excitations emitted by the impurity shown in Figure 4(g)–(h): at low speed, this wavevector is purely imaginary, so the collective excitation generated by the impurity does not transport momentum; at large speeds, instead, this wavevector acquires a finite real part, which is directly associated to the momentum dissipated by the impurity into the fluid.

Spatial structure of the condensate and supersolid behaviours. While thermodynamical arguments impose that equilibrium condensates form in the lowest-energy single-particle orbital [1,107], exciting features are observed in the spatial structure of finite-size nonequilibrium condensates. For instance, restricting the incoherent pump to a limited region of space allows to control the shape of the condensate via the so-called volcano effect: condensation mostly occurs

at the center of the pump spot, and then the coherent particles get expelled by the repulsive interactions and form a macroscopic outward-expanding radial flow. Originally observed in [108], this effect was theoretically interpreted in [109] and fully confirmed experimentally in [110].

While this is the typical behaviour of spatially homogeneous systems, even more intriguing phenomena are observed in spatially periodic lattice geometries [111]. Here, condensation into an excited state at the top of a photonic band is favoured by the interplay of a positive interaction energy and a negative effective mass which result in effectively attractive interactions. These keep the condensate localized in space with a soliton-like shape [112,113] and, in this way, reduce the condensation threshold with respect to condensation into the expanding positive-mass states at the bottom of the band.

A presently very active direction of research concerns the realization of quantum fluids of light that simultaneously display a long-range coherence and a spontaneously formed spatially periodic density modulation. This physics has been recently investigated in both theory and experiments [114,115] using devices displaying several photonic bands in the same energy range. While the main condensation process occurs at the top of a photonic band, a spatial modulation of the condensate density spontaneously appears as the result of coherent parametric scattering processes into finite wavevector modes in the side photonic bands. Such configurations can be seen as photonic analogs of the so-called supersolid states of matter as recently observed in atomic condensates [116].

With a proper design of the device geometry, e.g. in ring resonators, related parametric processes can be induced into modes at different frequencies: in this case, the density modulation continuously moves in space and gives temporally periodic oscillations in the emitted light intensity, while preserving a long-time phase coherence of the emission. The importance of such *optical comb generators* for a number of opto-electronic applications [117,118] suggests that the new insight on the stabilization of complex states of matter offered by the use of many-body physics concepts in the novel driven-dissipative context will open interesting perspectives also for opto-electronic technologies.

3.3.2. *Fluctuation and quasi-condensation effects*

Going beyond the mean-field approximation, it is interesting to look at the process of condensation from the point of view of statistical mechanics and, in particular, highlight the role of quantum and thermal fluctuations. In this context, a natural question is to assess under which conditions the nonequilibrium steady state can recover a thermal equilibrium case: as a general trend, a quasi-equilibrium state is approached if the rate of thermalizing collisions between particles within the fluid is faster than their decay rate [8]. While early works have assessed thermality in terms of the momentum distribution approaching or not a Bose–Einstein distribution at a well defined temperature[2] and chemical potential [119,120], recent works have highlighted the need to establish thermalization in terms of rigorous fluctuation-dissipation relations and frequency-dependent observables [121]. As we have mentioned from the beginning of this article, this departure from equilibrium is a key asset rather than a hindrance and underlies the exciting developments that we are reviewing here.

In full generality, condensation in a spatially uniform geometry is typically associated [1,107] to the appearance of a sharp and macroscopic $\mathbf{k} = 0$ peak in the momentum distribution $n(\mathbf{k}) = \langle \widehat{\widetilde{\Psi}}^{\dagger}(\mathbf{k})\, \widehat{\widetilde{\Psi}}(\mathbf{k}) \rangle$ where $\widetilde{\Psi}(\mathbf{k})$ is the Fourier transform of the quantum field $\widehat{\Psi}(\mathbf{r})$. Equivalently, from a

[2] Note that the fluid of light may well thermalize at a temperature different from the one of the solid-state device that is hosting it.

real-space perspective, condensation is instead signalled by the onset of long-range order in the correlation function

$$G^{(1)}(\mathbf{r},\mathbf{r}') = \left\langle \hat{\Psi}^{\dagger}(\mathbf{r})\,\hat{\Psi}(\mathbf{r}') \right\rangle \tag{50}$$

which tends to a non-zero value at long distances $|\mathbf{r}-\mathbf{r}'| \to \infty$ [122].

This criterion for condensation can be physically understood in analogy with ferromagnetism where the ferromagnetic transition is characterized in terms of the magnetization correlation function

$$G^{(1)}(\mathbf{r},\mathbf{r}') = \left\langle \vec{M}(\mathbf{r})\,\vec{M}(\mathbf{r}') \right\rangle. \tag{51}$$

In the high-temperature disordered state, the correlation function only displays short-range correlations and quickly tends to zero at long distances. On the other hand, long-range order is visible in the low-temperature ferromagnetic state where the correlation function tends to a finite value at long distances signalling a uniform magnetization throughout the whole system[3].

More formally, the SO(2) rotational symmetry that is spontaneously broken by the ferromagnetic transition of the xy model is mathematically equivalent to the $U(1)$ group describing the $\Psi \to \Psi\, e^{i\phi}$ symmetry that is spontaneously broken at the condensation transition. As the specific direction of the magnetization is randomly selected at every instance of the experiment, the average value of the magnetization $\vec{M}$ is zero by symmetry unless some external magnetic field is present to pin its direction. In this case, the reduced symmetry makes a gap to open in the dispersion of the soft magnon branch associated to the spontaneous symmetry breaking [123].

A similar phenomenon is expected to take place for the condensation phase transition: in the absence of external fields, the $U(1)$ symmetry guarantees the presence of a soft Goldstone mode such that $\lim_{k\to 0}\omega(k) = 0$ in both its real and imaginary parts. On the other hand, when the $U(1)$ symmetry is explicitly broken by some external field, a gap opens in the Goldstone mode dispersion. While particle-number conservation makes it difficult to verify this prediction in atomic condensates at equilibrium [124], the phase of an optical condensate can be pinned by an additional incident coherent laser [125] and a clear gap in the Goldstone mode dispersion is clearly observed in experiments [106]. Differently from the equilibrium case, however, the gap may open in the imaginary and/or in the real parts of the Goldstone mode dispersion depending on the specific system parameters.

Quasi-condensation effects in low-dimensions. While three-dimensional geometries are the most natural ones in condensed matter systems, standard optical systems are typically limited to a maximum of two dimensions. In analogy to the bounds imposed on phase transitions by the Hohenberg–Mermin–Wagner theorem of equilibrium statistical mechanics [107], it is then natural to wonder whether the reduced dimensionality has a similar impact also on the nonequilibrium phase transition. Even though the general theorem cannot be directly applied to the nonequilibrium context, specific calculations have predicted [126] that in one dimension the long range order does not survive the long-wavelength fluctuations and is replaced by an exponential decay of the same-time coherence, yet on relatively long distance scales. As a rough estimate, the fluctuations in this one-dimensional quasi-condensate can be interpreted as a temperature on the order of the loss rate $k_B T \sim \hbar\gamma$ [127]. Even more subtle features have been pointed out for the intermediate two-dimensional case where the Berezinskii–Kosterlitz–Thouless transition typical of equilibrium systems [128,129] may be replaced by a Kardar–Parisi–Zhang (KPZ) physics [130–132].

[3] It is interesting to note that a three-dimensional easy-plane (in the xy plane) model of ferromagnetism subject to an orthogonal magnetic field (along z) is expected to display a steady rotation of the magnetization rotation along z. As a result, the x and y components of the magnetization display monochromatic oscillations as it happens to the field ψ of the optical model.

A common tool for the theoretical study of these phenomena is offered by the stochastic Gross–Pitaevskii equation discussed in Section 3.1.2. From an experimental standpoint, a very important asset for the study of the critical properties and of the spatio-temporal correlation function in the different regimes is provided by the radiative loss channel: as the coherence properties of the in-cavity field are imprinted into the one of the emitted radiation, their measurement can be straightforwardly performed with standard optical techniques. This feature has been exploited in experimental studies of the correlation properties across the phase transition and, in particular, for the recent observation of KPZ universal behaviours in a one-dimensional configuration [133].

While moving up to two-dimensional systems is not expected to pose additional conceptual challenges to optical experiments, three- and higher-dimensional configurations require the use of synthetic dimension schemes where extra spatial dimension are encoded in some other degrees of freedom of the photon, e.g. the different cavity modes of a ring resonator [134–136]. Pioneering experimental work on the collective dynamics arising from the combination of gain with one synthetic dimension in a ring laser was reported in [137,138]; an extension to a topological two-dimensional array of coupled ring resonators was presented in [139]. As next steps, we anticipate the possibility of extending this idea to study condensation in novel high-dimensional contexts and, in this way, unveil peculiar statistical behaviours resulting from the interplay of KPZ physics with the roughening transition [140–143].

4. Strongly correlated systems

In the previous sections we have discussed the physics of dilute driven-dissipative systems: for sufficiently weak interactions, a mean-field theory based on (stochastic) partial differential equations for classical fields provides an accurate description of the steady-state and of the dynamics of the system. In this last section, we briefly summarize the state-of-the-art and some future developments in the direction of realizing strongly correlated states of photonic matter that can be observed in systems with strong optical nonlinearities.

4.1. *Coherent drive*

4.1.1. *Photon blockade in a single-mode cavity*

The first proposal in this direction [144] was the so-called *photon blockade* effect. The dynamics of the quantum electromagnetic field in a nonlinear single-mode cavity can be described by a nonlinear oscillator Hamiltonian of the form

$$H = \hbar\omega_o \hat{a}^\dagger \hat{a} + \frac{\hbar\omega_{\rm nl}}{2} \hat{a}^\dagger \hat{a}^\dagger \hat{a}\hat{a} \tag{52}$$

where the anharmonicity is quantified by the parameter $\omega_{\rm nl}$ proportional to the $\chi^{(3)}$ optical nonlinearity of the nonlinear medium embedded in the cavity. In a planar geometry, we can make use of (15) to get

$$\omega_{\rm nl} = \frac{g_{\rm nl}}{\mathscr{S}} \tag{53}$$

where the effective mode area $\mathscr{S}$ is defined as

$$\mathscr{S} = \frac{\left(\int \mathrm{d}^2\mathbf{r}_\parallel \left|\mathscr{E}_\parallel(\mathbf{r}_\parallel)\right|^2\right)^2}{\int \mathrm{d}^2\mathbf{r}_\parallel \left|\mathscr{E}_\parallel(\mathbf{r}_\parallel)\right|^4} \tag{54}$$

in terms of the mode profile $\mathscr{E}_\parallel(\mathbf{r}_\parallel)$ along the cavity plane.

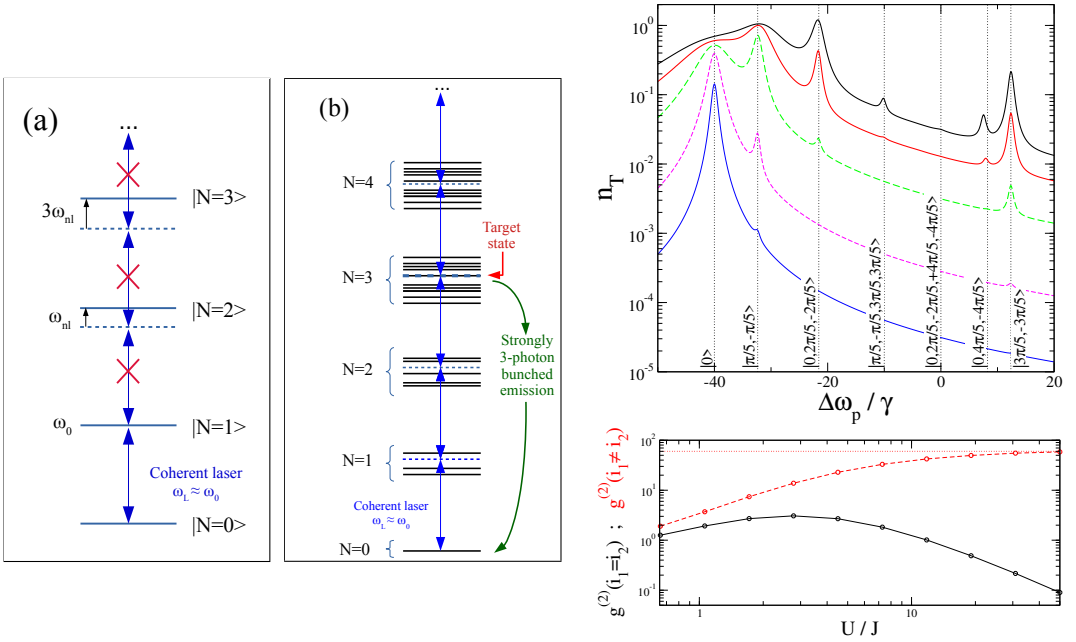

Figure 5. Left panel (a): sketch of the photon blockade mechanism for a single-mode cavity under a coherent pumping exactly on resonance with the bare cavity frequency, $\omega_{\rm inc} = \omega_o$. Because of the strong nonlinearity $\omega_{\rm nl} \gg \gamma_{\rm loss}$, transitions to all $N > 1$ states are non-resonant and the dynamics is confined to the $N = 0, 1$ states, giving effectively impenetrable photons. Central panel (b): sketch of the coherent pumping scheme to selectively excite a $N = 3$-photon state via a three-photon transition. Top-right panel: generation of a Tonks–Girardeau gas of fermionized photons under coherent pumping. Spectrum of total photon number n_T as a function of the incident frequency $\Delta\omega_p = \omega_{\rm inc} - \omega_o$ for different values of the pump intensity, $F/\gamma_{\rm loss} = 0.1, 0.3, 1, 2, 3$. Photons are assumed to be perfectly impenetrable $U/\gamma_{\rm loss} = \infty$ and losses small enough to resolve many-body states $J/\gamma_{\rm loss} = 20$. The vertical dotted lines indicate the theoretical prediction for the position of the N-photon resonance peak corresponding to each many-body state; the label indicates the orbitals filled in the corresponding fermionic wavefunction. Bottom-right panel: second order photon correlations in the emission from the same (black) and from different (red) sites as a function of the interaction constant $\omega_{\rm nl}/\gamma_{\rm loss}$. At each point, the coherent drive is set on resonance with the lowest two-photon state of a 3-sites chain. The right panels are adapted from [145].

Independently of the specific geometry, the eigenstates of (52) are labelled by the photon number and have an energy

$$E_n = n\hbar\omega_o + \hbar\omega_{\rm nl}\frac{n(n-1)}{2}. \tag{55}$$

As it is sketched in the left-most panel of Figure 5, the energy separation $E_{n+1} - E_n = \hbar\omega_o + n\hbar\omega_{\rm nl}$ is a growing function of n. As such, a coherent incident field resonant with the $0 \to 1$ transition will not be able to further excite the system to the $n \geq 2$ states as the corresponding transitions are no longer resonant. For instance, the $1 \to 2$ transition is detuned by an effective interaction energy $\omega_{\rm nl}$: as soon as this exceeds the cavity linewidth $\omega_{\rm nl} \gg \gamma_{\rm loss}$, the coherent field is not able to efficiently drive this second transition, so the cavity system ends up behaving as an effective

two-level system. In physical terms, this can be understood as photons becoming effectively impenetrable objects, a situation that is in stark contrast with the prediction of the linear Maxwell equations where photons are rigorously non-interacting particles.

4.1.2. *Many-body states*

A straightforward generalization of this pumping scheme can be exploited to generate strongly correlated many-photon states in spatially extended geometries such as cavity arrays. The key idea, sketched in the central panel of Figure 5, is to resonantly drive a N-photon transition to bring the system from its zero-photon vacuum state to the desired N-photon eigenstate of the conservative many-body Hamiltonian: the crucial requirement for an efficient selectivity of this preparation scheme is that the energy gap between the desired N-photon eigenstate and its neighbors exceeds the linewidth of the N-photon states, which typically grows as $N\gamma_{\rm loss}$.

As a first example, this idea was theoretically explored in view of realizing a Tonks–Girardeau gas of impenetrable photons in a one-dimensional chain of coupled cavities [145]. This is described by a Hamiltonian in the form

$$H = \sum_j \hbar\omega_o \hat{a}_j^\dagger \hat{a}_j + \frac{\hbar\omega_{\rm nl}}{2} \hat{a}_j^\dagger \hat{a}_j^\dagger \hat{a}_j \hat{a}_j - \hbar J \sum_{\langle j,j'\rangle} \hat{a}_j^\dagger \hat{a}_{j'} \tag{56}$$

where the indices j, j' run over the sites of the chain, assumed to have periodic boundary conditions, and the hopping terms of amplitude $J > 0$ are restricted to next-neighbor sites. The impenetrability condition is enforced by assuming $\omega_{\rm nl} \gg J$. A coherent pump is assumed to drive all sites according to the discrete version of (18),

$$H_{\rm coh} = \hbar \sum_j \left[F_j(t)\, \hat{a}_j^\dagger + \hbar F_j(t)^*\, \hat{a}_j \right]. \tag{57}$$

In what follows, we assume that all sites are driven in a monochromatic way with the same amplitude F and frequency $\omega_{\rm inc}$, that is $F_j(t) = F\, e^{-i\omega_{\rm inc} t}$. As the master equation is in the Lindblad form, the steady-state and the dynamics of the system can be calculated with standard numerical tools, e.g. by projecting the master equation on the basis of number states. Note that efficient high-level numerical libraries are nowadays available for these tasks [146].

Examples of spectra of the steady-state total population $n_T = \sum_j \langle \hat{a}_j^\dagger \hat{a}_j \rangle$ as a function of the incident frequency $\omega_{\rm inc}$ are shown in the upper-right panel of Figure 5 for growing values of the incident intensity $|F|^2$: at low intensity (blue line), the spectrum is characterized by a single main peak corresponding to the 1-photon transition to the $k = 0$ orbital. At growing intensities, additional peaks at frequencies corresponding to the higher $N = 2, 3, \ldots$ photon transitions appear. As expected, the position of each of these peaks matches the frequency of the N-photon resonance from the vacuum state (at zero energy) to some N-photon state of energy ω_N^α within the $k = 0$ sector,

$$\omega_{\rm inc} = \omega_N^\alpha / N. \tag{58}$$

In the specific Tonks–Girardeau case, the different excited states are labeled by the quasi-momenta of the (fermionized) particles and their energy can be analytically calculated [147]. The expected position of the resonances is indicated in the Figure by the vertical lines, which indeed match well with the position of the numerically calculated resonance peaks.

In order to be able to selectively drive the desired many-body state, the frequency separation from the neighboring states has to exceed the linewidth: as the separation is typically set by the hopping J and interaction $\omega_{\rm int}$ energies and the broadening grows as $N\gamma_{\rm loss}$, the requirement on the linewidth $\gamma_{\rm loss}$ becomes more and more stringent as larger N states are targeted. On top of this, one must not forget that for growing values of the drive amplitude F, each peak eventually displays a sizable power-broadening on top of its natural linewidth.

As it is well known from atomic physics [148], a coherent illumination leads to a reversible oscillatory dynamics between the different states, with absorption processes followed by stimulated emission ones until a steady-state is enforced via spontaneous emission processes. In particular, for very strong incident intensities, the steady-state tends to an equidistribution of the population among the different states. As such, a continuous-wave excitation can hardly be used to transfer all the population to a given excited state, but more complex pulsed schemes have to be adopted to generate, e.g., a state with a well-defined N.

Nonetheless, as the steady-state population of many-body states is typically a decreasing function of their photon number N, this difficulty can be circumvented by specifically looking at N-photon observables. Such observables are in fact strictly zero on all lower $N' < N$ photon states and, up to moderate values of the incident intensity, only receive a sub-dominant contribution from the higher $N' > N$ ones. A concrete example of application of this idea is illustrated in the bottom-right panel of Figure 5, where we specifically look at $N = 2$ observables such as the second-order correlation function of the emission

$$g^{(2)}(i_1, i_2) = \frac{\langle \hat{a}^\dagger_{i_1} \hat{a}^\dagger_{i_2} \hat{a}_{i_2} \hat{a}_{i_1} \rangle}{\langle \hat{a}^\dagger_{i_1} \hat{a}_{i_1} \rangle \langle \hat{a}^\dagger_{i_2} \hat{a}_{i_2} \rangle}. \tag{59}$$

Depending on the relative value of the interaction and hopping parameters $\omega_{\rm nl}/J$, the $N = 2$-photon eigenstates go from being delocalized, approximately non-interacting-photon states to fermionized, impenetrable-photon states. This key difference directly translate to the shape of $g^{(2)}(i_1, i_2)$: for non-interacting photons it has a position-independent value equal to 1; for impenetrable photons, its same-point value is much suppressed with respect to its different-point value, $g^{(2)}(i_1 = i_2) \ll g^{(2)}(i_1 \neq i_2)$. This illustrates how a coherent drive followed by a measurement of a N-photon correlation function allows to obtain interesting information on the many-body eigenstates of a strongly interacting system. A conceptually related experiment was reported using a superconducting circuit-QED platform in [149].

Further theoretical work [150] has extended this idea to a two-dimensional lattice geometry where impenetrable photons are also subject to a synthetic magnetic field. In this geometry, the optical transitions occur from the vacuum state to strongly correlated N-photon states analogous to the ones of fractional quantum Hall systems. An example of the peculiar physics of this regime is illustrated in the top-left panel (a) of Figure 6. Here, we show how tuning the coherent pump frequency on the lowest $N = 2$-photon resonance peak, one can extract information on the complex microscopic structure of the Laughlin states from the two-photon correlations of the emitted light: even in a small 4×4 lattice, we recognize in the wavefunction a clear antibunching feature between pairs of strongly interacting photons as well as a complex phase profile as a function of the relative position.

A closely related idea has been experimentally explored in a recent experiment [152]: strong interactions between photons are obtained by coupling light to optically dressed atoms in a Rydberg-EIT configuration [31,153]; a synthetic magnetic field in a cylindrically symmetric geometry is obtained by using a twisted optical ring-cavity [154]. Combining these elements, a two-photon Laughlin state is selectively created using a coherent laser pump with finite angular momentum and its microscopic structure is probed by looking at the correlation functions of the emitted light at different spatial positions and in different orbital angular momentum channels.

Scaling up the idea to larger photon numbers is naturally the next goal, but several challenges are still present along this way. As it was mentioned above, an obvious difficulty comes from the decreasing value of the spacing between many-body resonances which imposes stricter constraints on their linewidth. An even more serious challenge comes from the quickly decreasing value of the matrix element for driving a N-photon transition from the trivial vacuum state to a topologically non-trivial FQH state with a coherent light beam formed by uncorrelated photons.

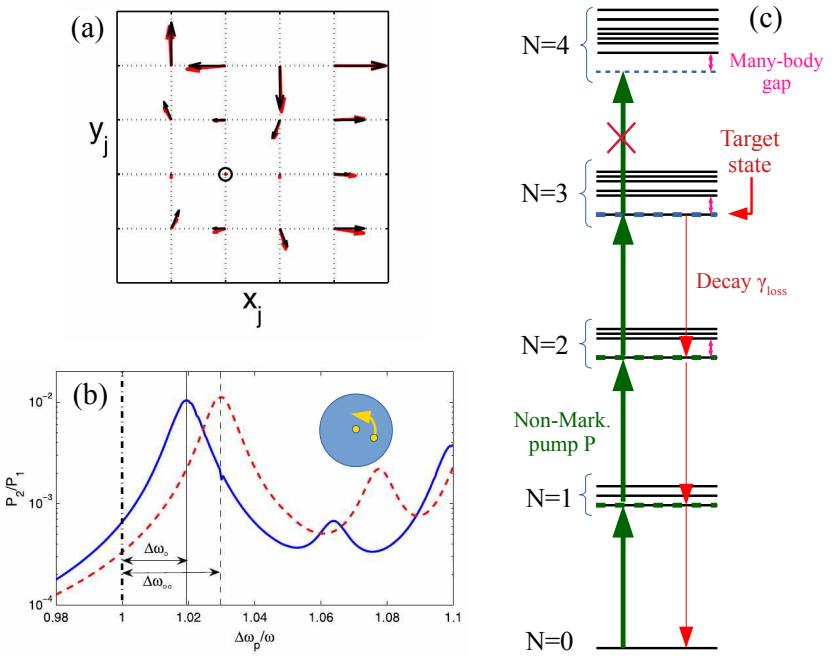

Figure 6. Top-left panel (a): reconstruction of the two-particle wavefunction of a Laughlin state from the two-photon correlations of the light emitted by the two-photon FQH state generated under coherent pumping. The marker indicates the position of one photon; the x_j, y_j coordinates on the plot correspond to the second photon's position: the red arrows indicate the two-photon emission amplitude, the black ones indicate the value of the complex-valued Laughlin wavefunction discretized in the lattice. Bottom-left panel (b): frequency-shift of the two-photon resonance peak under the effect of the braiding of a quasi-hole. The continuous blue line is the spectrum for a single quasi-hole braided around the cloud at a radius $r/\ell = 0.4$; the dashed red line spectrum includes also a stationary second hole located at $r = 0$, as indicated in the sketch in the inset. Right panel (c): sketch of the frequency-selective incoherent pumping scheme to stabilize a $N = 3$ FQH state. The non-Markovian nature of the pump prevents excitation across the many-body gap. The (Markovian) photon losses cannot lead to states above the many-body gap. All together, this restricts the dynamics to states with $N \leq 3$ photons below the many-body gap. Panel (a) is adapted from [150]. Panel (b) is adapted from [151].

4.1.3. *Signatures of the braiding phase*

In spite of these difficulties, an intriguing new possibility offered by the driven-dissipative condition is illustrated in the bottom-left panel (b) of Figure 6. One of the key feature of a topological state of matter is encoded in the so-called *braiding phase* that the many-body wavefunction acquires when two quasi-holes are made to adiabatically move through the fluid and encircle each other as sketched in the inset. While the braiding phase is a mathematically well defined concept [101,155], an experimental observation of the overall phase of a quantum wavefunction requires to design some interference process between different quantum states [156–158]. Quan-

tum superpositions of the vacuum state and the desired many-body state are naturally generated by a coherent pumping process, so any extra phase acquired by the many-body wavefunction may be observed as a shift in the resonance frequency of the corresponding transition.

A concrete implementation of this general idea to measure the braiding phase in driven-dissipative fractional quantum Hall fluids of light was proposed in [151]. In the presence of one or more localized repulsive potentials, the lowest energy two-photon eigenstate consists of a Laughlin state pierced by quasi-holes pinned at the position of the potentials. When a single quasi-hole is braided around the fluid at a radius r_o from the center with a constant angular velocity Ω, the many-body wavefunction acquires at each roundtrip a phase given by the flux of synthetic magnetic field enclosed by the trajectory. This phase, of geometric origin, is responsible for the shift $\Delta\omega_o$ of the main $N=2$-photon peak visible on the blue spectrum of Figure 6(b). When a second hole is present at the origin, the shift $\Delta\omega_{oo}$ acquires an additional contribution due to the braiding of one quasi-hole around the other,

$$\Delta\omega_{oo} - \Delta\omega_o = \varphi_{Br}\frac{\Omega}{2\pi}. \tag{60}$$

where φ_{Br} is the braiding phase accumulated at each round trip and $2\pi/\Omega$ is the time needed for a round-trip. The frequency shift observed in the numerical simulation in Figure 6(b) is in excellent agreement with the value theoretically extracted from a microscopic calculation of the many-body braiding phase for this configuration. As it is discussed in detail in [151], the value of the braiding phase tends to the topological value π as soon as the cloud has a macroscopic size and edge effects can be neglected. In principle this requires a number $N \gg 1$ of particles; interestingly in view of experiments, a qualitative effect is already visible for $N=3$ and the asymptotic value is closely approached for $N\sim 10$.

This theoretical prediction shows how the quantum superposition nature of the state that is naturally generated in a coherent pumping process is not only a limitation of the preparation process, but can be exploited as a new asset to observe the peculiar properties of the many-body wavefunction of topological states of matter.

4.2. *Incoherent pumping*

In the previous subsection we have seen how the reversible nature of the coherent pumping process makes the driven-dissipative steady-state to typically consist of a superposition of different number states. If one wishes to concentrate the population on a single excited state, many-photon generalizations of the π-pulses used in the coherent manipulation of the internal state of atoms [148] can be envisaged. As the many-body states are very close in energy, sophisticated quantum control techniques may be required to achieve a good selectivity, which furthermore rely on some preliminary theoretical knowledge of the system.

An alternative way, inspired to population inversion in laser physics, is to exploit an incoherent pumping scheme to irreversibly push the population upwards towards higher-N states. In its simplest formulation with a broad-band incoherent pump as described within the Markovian setting of (19), this incoherent pump scheme allows to efficiently push the population upwards but the absence of energy-selectivity makes the population spread among the different many-body states forming each N-photon manifold, typically in a uniform way [59]. As a result, the fluid ends up displaying an effectively infinite temperature which prevents observation of interesting quantum many-body effects.

A promising way-out is to introduce a frequency-selectivity of the pumping scheme which provides non-Markovian features in the irreversible coupling between the system and the external bath used for pumping. A simple implementation of this idea is sketched in the right panel

of Figure 6 in the context of generating a FQH fluid of light: provided the spectrum of the incoherent pump is narrower than the many-body gap protecting the target FQH state, the pumping cannot lead to states above the many-body gap. As states above the many-body gap cannot be reached by loss processes either[4], the population remains concentrated within the states below the many-body gap. If the geometry of the fluid has periodic boundary conditions, the incompressibility of the bulk puts an upper bound to the number of particles that can be accommodated in a non-interacting state before one has to cross the many-body energy gap, e.g. a maximum of $N = 3$ particles for the configuration illustrated in the sketch. If the incoherent pumping rate $\gamma_{\rm pump}$ exceeds the loss rate $\gamma_{\rm loss}$, the population is irreversibly pushed up along the ladder of N states and gets eventually concentrated in the upmost available state which is indeed our target FQH state.

The situation is slightly more complicate if the periodic boundary conditions are replaced by a finite geometry with physical edges, e.g., when the fluid is subject to a confining potential [159] or has open boundary conditions [160,161]. In these cases, the energy gap to the lowest edge excitation is typically much smaller than the many-body gap in the bulk and scales inversely to the cloud perimeter. This puts more and more severe constraints on the energy selectivity of the pumping process that is required to suppress spurious edge excitations. However, since these excitations are confined on the edge of the cloud, they do not create any harm to the topological properties of the bulk which remains well stabilized in a very pure fractional quantum Hall state.

In order to put these qualitative arguments onto solid and quantitative grounds one needs to develop a theoretical description that is able to account for the non-Markovian features associated to the frequency-dependence of the pumping process. In [62,162], this was done by explicitly introducing into the model two-level emitters that provide a frequency-dependent injection of photons as discussed at the beginning of Section 2.2.4. This allows to reformulate the frequency-dependent incoherent pumping in terms of a master equation in the Lindblad form, which can then be solved with standard methods, e.g. using one of the numerical libraries that are available for these tasks [146]. In the fast repumping regime where the emitters can be adiabatically eliminated, a simplified photon-only description based on generalized Lindblad master equation can be used, as presented in Section 2.2.4. This has provided interesting insight both in lattice and in continuum geometries [63,163]. On top of these numerical works, some analytical results have also been obtained in specific limiting cases [164], further confirming the promise of this framework for the autonomous stabilization of FQH states. On top of these feasibility studies, interesting consequences of the driven-dissipative nature of the fluid have also been pointed out in theoretical works. While isolated quasi-holes in the bulk of a standard equilibrium FQH fluid move along deterministic trajectories, typically with very low speeds, a recent work [165] has anticipated that repeated loss and repumping processes in the neighborhood of a quasi-hole give rise to an effectively stochastic motion of quasi-holes.

The conceptual facility of this mechanism for the *autonomous stabilization* of a fractional quantum Hall fluid of light is a consequence of the peculiar structure of the many-body spectrum and of the many-body eigenstates. Something similar occurs for the deep Mott insulator state,

[4] This is easy to see on the analytical form of the Laughlin wavefunctions of FQH states [101],

$$\psi(z_1,\dots,z_N) = P(z_1,\dots,z_N) \prod_{i>j} (z_i - z_j)^p \, e^{-\sum_i |z_i|^2},$$

where P is an arbitrary symmetric polynomial in the normalized complex $z_i = (x_i + i\, y_i)/\ell_B$ coordinates of the $i = 1,\dots,N$ particles and p is an integer (even for bosonic particles like photons and odd for fermionic particles like electrons) characterizing the specific FQH state under consideration. The non-interacting nature of this state is enforced by the presence of factors $(z_i - z_j)$ for any pair i, j of particles, which give zeros in the wavefunction for overlapping particles. This impenetrability condition is preserved when a particle is removed from the system.

whose stabilization was experimentally demonstrated [64] using a superconductor-based circuit-QED platform operating in the $\omega_{\rm nl} \gg J$ regime (in the notation of the lattice Hamiltonian (56)). In this limit, the thickness of the band of hole states (on the order of J) is much smaller than the energy separation (on the order of $\omega_{\rm nl}$) from excited states featuring some doubly occupied site: choosing a repumping rate $J \ll \Gamma_P \ll \omega_{\rm nl}$ then guarantees an effective replenishing of any hole, while suppressing the creation of unwanted doublons.

An even richer physics occurs when J and $\omega_{\rm nl}$ have comparable values, so that the driven-dissipative condition interplays with the superfluid-insulator quantum phase transition occurring at a finite critical value of $J/\omega_{\rm nl}$ [3]. In [166,167], a square-like form of the incoherent emission spectrum, arising e.g. from an inhomogeneously broadened distribution of emitters, was considered, that leads to an equilibrium-like superfluid-insulator transition. The case of a Lorentzian spectrum was instead considered in [162] and specific nonequilibrium features were pointed out for the superfluid-insulator transition. Beyond the steady-state, the spectrum of the collective excitations on top of the driven-dissipative steady state was studied across the different regimes in [62]: similarly to the equilibrium case, gapped particle-hole excitations are found in the insulating state and a gapless Goldstone mode in the superfluid state. As a typical feature of driven-dissipative systems, this latter was predicted to have the same diffusive properties as in the weakly-interacting case discussed in Section 3.3.

5. Conclusions and perspectives

In this article we have reviewed the basic concepts of the driven-dissipative many-body physics of quantum fluids of light and we have summarized the main theoretical tools used for their description. A special emphasis has been given to those new effects and those new tools that the driven-dissipative nature introduces for the stabilization and the manipulation of interesting states of photonic matter.

As illustrative examples, in the weakly interacting regime, a suitable coherent pump can be used to generate inhomogeneous flows displaying acoustic horizons; in topological photonic systems, the interplay between the bandwidth of energy bands and the loss rate can be exploited to smoothly transition from an anomalous Hall to a quantum integer Hall regime in the transverse drift under crossed synthetic magnetic and electric fields. In the strongly interacting regime, spectroscopical signatures of the anyonic braiding phase in fractional quantum Hall fluids of light have been anticipated under coherent pumping and promising incoherent pumping schemes to stabilize macroscopic strongly correlated fluids are being actively investigated.

These advances are opening exciting perspectives in a number of interdisciplinary directions, at the crossroad of many-body physics, nonlinear statistical mechanics, and quantum simulation of gravitational problems. As we have mentioned along the article, acoustic horizons in inhomogeneous flows have been predicted to give acoustic analogs of Hawking radiation, which could be experimentally detected in the intensity correlations of the emitted light. The flexibility in the generation and the manipulation of different flow geometries is of utmost interest in view of studying more complex phenomena where, e.g., Hawking radiation interplays with superradiance and localized quasi-normal modes [168] of the underlying space-time. The coherence properties of condensates and quasi-condensates display universality features that fall in the framework of the Kardar–Parisi–Zhang framework: going beyond the one-dimensional geometries considered so far in experiments, the combination of condensation with synthetic dimensions opens the way to studies of nonequilibrium statistical mechanics and many-body effects in high dimensional geometries beyond the three dimensions of our physical space [169]. Finally, application of the frequency-dependent incoherent pumping techniques to strongly interacting photons in

complex geometries and/or in the presence of non-trivial band topologies offers promising avenues towards the driven-dissipative stabilization of strongly correlated states of photonic matter and the observation of their peculiar collective excitations, including those Abelian and non-Abelian anyonic statistics that are of interest for topological quantum computing [170].

Beyond quantum fluids of light, driven-dissipative schemes are presently attracting a growing interest also in the context of ultracold atomic gases. A well-established direction is to design dissipation channels that tend to push the atomic gas towards a desired many-body state [10–15]. A more recent research avenue focuses on configurations where a net particle flux is established by letting the system exchange atoms with several suitably designed reservoirs, either in an incoherent way via inter-atomic collisions or in a coherent way via internal transitions driven by incident electromagnetic fields. Examples of this strategy are the engineered evaporation leading to condensation into a (topological) excited state observed in [171] and, even more directly, the continuously loaded Bose–Einstein condensate that was generated in the driven-dissipative steady-state of a complex atom cooling apparatus in [16]. Taking inspiration from fluids of light [106,133], a natural next question is to explore the consequences of the nonequilibrium nature on the coherence and on the collective modes of the driven-dissipative atomic condensate. On the coherent pumping side, macroscopic atomic reservoirs involving a condensate have been used to realize atomic analogs of the coherent pumping schemes: first experiments have demonstrated bistability effects in single mode geometries [17,18]; along the lines of the recent experiments demonstrating baby fractional quantum Hall fluids of light [152], analogous work is in progress in the direction of stabilizing strongly correlated states of atomic matter.

Declaration of interests

The author does not work for, advise, own shares in, or receive funds from any organization that could benefit from this article, and has declared no affiliations other than their research organizations.

References

[1] L. P. Pitaevskiĭ and S. Stringari, *Bose–Einstein condensation and superfluidity*, International Series of Monographs on Physics, Oxford University Press, 2016, 512 pages.

[2] C. Gross and I. Bloch, "Quantum simulations with ultracold atoms in optical lattices", *Science* **357** (2017), no. 6355, pp. 995–1001.

[3] I. Bloch, J. Dalibard and W. Zwerger, "Many-body physics with ultracold gases", *Rev. Mod. Phys.* **80** (2008), no. 3, pp. 885–964.

[4] N. R. Cooper, J. Dalibard and I. B. Spielman, "Topological bands for ultracold atoms", *Rev. Mod. Phys.* **91** (2019), no. 1, article no. 015005.

[5] I. Carusotto and C. Ciuti, "Quantum fluids of light", *Rev. Mod. Phys.* **85** (2013), no. 1, pp. 299–366.

[6] D. E. Chang, V. Vuletić and M. D. Lukin, "Quantum nonlinear optics – photon by photon", *Nature Photon.* **8** (2014), no. 9, pp. 685–694.

[7] I. Carusotto, A. A. Houck, A. J. Kollár, P. Roushan, D. I. Schuster and J. Simon, "Photonic materials in circuit quantum electrodynamics", *Nat. Phys.* **16** (2020), no. 3, pp. 268–279.

[8] J. Bloch, I. Carusotto and M. Wouters, "Non-equilibrium Bose–Einstein condensation in photonic systems", *Nat. Rev. Phys.* **4** (2022), no. 7, pp. 470–488.

[9] L. M. Sieberer, M. Buchhold and S. Diehl, "Keldysh field theory for driven open quantum systems", *Rep. Prog. Phys.* **79** (2016), no. 9, article no. 096001.

[10] S. Diehl, A. Micheli, A. Kantian, B. Kraus, H. P. Büchler and P. Zoller, "Quantum states and phases in driven open quantum systems with cold atoms", *Nat. Phys.* **4** (2008), no. 11, pp. 878–883.

[11] C.-E. Bardyn, M. A. Baranov, E. Rico, A. Imamoğlu, P. Zoller and S. Diehl, "Majorana modes in driven-dissipative atomic superfluids with a zero Chern number", *Phys. Rev. Lett.* **109** (2012), article no. 130402.

[12] J. C. Budich, P. Zoller and S. Diehl, "Dissipative preparation of Chern insulators", *Phys. Rev. A* **91** (2015), article no. 042117.

[13] F. Mivehvar, F. Piazza, T. Donner and H. Ritsch, "Cavity QED with quantum gases: new paradigms in many-body physics", *Adv. Phys.* **70** (2021), no. 1, pp. 1–153.

[14] F. Ferri, R. Rosa-Medina, F. Finger, N. Dogra, M. Soriente, O. Zilberberg, T. Donner and T. Esslinger, "Emerging dissipative phases in a superradiant quantum gas with tunable decay", *Phys. Rev. X* **11** (2021), article no. 041046.

[15] B. P. Marsh, R. M. Kroeze, S. Ganguli, S. Gopalakrishnan, J. Keeling and B. L. Lev, "Entanglement and replica symmetry breaking in a driven-dissipative quantum spin glass", *Phys. Rev. X* **14** (2024), no. 1, article no. 011026.

[16] C.-C. Chen, R. González Escudero, J. Minář, B. Pasquiou, S. Bennetts and F. Schreck, "Continuous Bose–Einstein condensation", *Nature* **606** (2022), no. 7915, pp. 683–687.

[17] R. Labouvie, B. Santra, S. Heun and H. Ott, "Bistability in a driven-dissipative superfluid", *Phys. Rev. Lett.* **116** (2016), article no. 235302.

[18] J. Benary, C. Baals, E. Bernhart, J. Jiang, M. Röhrle and H. Ott, "Experimental observation of a dissipative phase transition in a multi-mode many-body quantum system", *New J. Phys.* **24** (2022), no. 10, article no. 103034.

[19] Q. Glorieux, C. Piekarski, Q. Schibler, T. Aladjidi and M. Baker-Rasooli, "Paraxial fluids of light", preprint, 2025. Online at https://arxiv.org/abs/2504.06262.

[20] C. Michel, O. Boughdad, M. Albert, P.-É. Larré and M. Bellec, "Superfluid motion and drag-force cancellation in a fluid of light", *Nat. Commun.* **9** (2018), no. 1, pp. 1–6.

[21] Q. Fontaine, T. Bienaimé, S. Pigeon, É. Giacobino, A. Bramati and Q. Glorieux, "Observation of the Bogoliubov dispersion in a fluid of light", *Phys. Rev. Lett.* **121** (2018), no. 18, article no. 183604.

[22] P. Coullet, L. Gil and F. Rocca, "Optical vortices", *Opt. Commun.* **73** (1989), no. 5, pp. 403–408.

[23] M. Vaupel, K. Staliunas and C. O. Weiss, "Hydrodynamic phenomena in laser physics: modes with flow and vortices behind an obstacle in an optical channel", *Phys. Rev. A* **54** (1996), pp. 880–892.

[24] M. Baker-Rasooli, T. Aladjidi, N. A. Krause, A. S. Bradley and Q. Glorieux, "Observation of Jones–Roberts solitons in a paraxial quantum fluid of light", *Phys. Rev. Lett.* **134** (2025), article no. 233401.

[25] M. Baker-Rasooli, W. Liu, T. Aladjidi, A. Bramati and Q. Glorieux, "Turbulent dynamics in a two-dimensional paraxial fluid of light", *Phys. Rev. A* **108** (2023), article no. 063512.

[26] T. D. Ferreira, J. Garwoła and N. A. Silva, "Exploring the dynamics of the Kelvin–Helmholtz instability in paraxial fluids of light", *Phys. Rev. A* **109** (2024), no. 4, article no. 043704.

[27] K. Baudin, A. Fusaro, K. Krupa, J. Garnier, S. Rica, G. Millot and A. Picozzi, "Classical Rayleigh–Jeans condensation of light waves: observation and thermodynamic characterization", *Phys. Rev. Lett.* **125** (2020), article no. 244101.

[28] K. Krupa, A. Tonello, B. M. Shalaby, M. Fabert, A. Barthélémy, G. Millot, S. Wabnitz and V. Couderc, "Spatial beam self-cleaning in multimode fibres", *Nature Photon.* **11** (2017), no. 4, pp. 237–241.

[29] A. Chiocchetta, P.-É. Larré and I. Carusotto, "Thermalization and Bose–Einstein condensation of quantum light in bulk nonlinear media", *Eur. Phys. Lett.* **115** (2016), no. 2, article no. 24002.

[30] J. Steinhauer et al., "Analogue cosmological particle creation in an ultracold quantum fluid of light", *Nat. Commun.* **13** (2022), no. 1, pp. 1–7.

[31] T. Peyronel, O. Firstenberg, Q.-Y. Liang, S. Hofferberth, A. V. Gorshkov, T. Pohl, M. D. Lukin and V. Vuletić, "Quantum nonlinear optics with single photons enabled by strongly interacting atoms", *Nature* **488** (2012), no. 7409, pp. 57–60.

[32] O. Firstenberg, T. Peyronel, Q.-Y. Liang, A. V. Gorshkov, M. D. Lukin and V. Vuletić, "Attractive photons in a quantum nonlinear medium", *Nature* **502** (2013), no. 7469, pp. 71–75.

[33] A. V. Kavokin, J. J. Baumberg, G. Malpuech and F. P. Laussy, *Microcavities*, revised edition, Oxford Science Publications, Oxford University Press, 2011, 488 pages.

[34] J. D. Jackson, *Classical electrodynamics*, 3rd edition, John Wiley & Sons, 1999.

[35] W. Heisenberg and H. Euler, "Folgerungen aus der Diracschen Theorie des Positrons", *Z. Phys.* **98** (1936), no. 11, pp. 714–732.

[36] E. Lundström, G. Brodin, J. Lundin, M. Marklund, R. Bingham, J. Collier, J. T. Mendonça and P. Norreys, "Using high-power lasers for detection of elastic photon-photon scattering", *Phys. Rev. Lett.* **96** (2006), article no. 083602.

[37] D. Micieli et al., "Compton sources for the observation of elastic photon-photon scattering events", *Phys. Rev. Accel. Beams* **19** (2016), no. 9, article no. 093401.

[38] E. Milotti et al., "Exploring quantum vacuum with low-energy photons", *Int. J. Quantum Inf.* **10** (2012), no. 08, article no. 1241002.

[39] K. I. Beloborodov, T. A. Kharlamova and V. I. Telnov, "Problems of studying $\gamma\gamma \to \gamma\gamma$ scattering at e^+e^- and $\gamma\gamma$ colliders", preprint, 2023. Online at https://arxiv.org/abs/2301.07089.

[40] ATLAS Collaboration, "Evidence for light-by-light scattering in heavy-ion collisions with the ATLAS detector at the LHC", *Nat. Phys.* **13** (2017), no. 9, pp. 852–858.

[41] N. W. Ashcroft and N. D. Mermin, *Solid state physics*, Cengage Learning, Cengage, 2022.

[42] P. N. Butcher and D. Cotter, *The elements of nonlinear optics*, Cambridge Studies in Modern Optics, Cambridge University Press, 2008, xiv+344 pages.

[43] R. W. Boyd, *Nonlinear optics*, Academic Press Inc., 2008, xix+613 pages.

[44] A. Blais, A. L. Grimsmo, S. M. Girvin and A. Wallraff, "Circuit quantum electrodynamics", *Rev. Mod. Phys.* **93** (2021), article no. 025005.

[45] S. Ferretti and D. Gerace, "Single-photon nonlinear optics with Kerr-type nanostructured materials", *Phys. Rev. B* **85** (2012), article no. 033303.

[46] B. Nelsen, G. Liu, M. Steger, D. W. Snoke, R. Balili, K. West and L. N. Pfeiffer, "Dissipationless flow and sharp threshold of a polariton condensate with long lifetime", *Phys. Rev. X* **3** (2013), no. 4, article no. 041015.

[47] Y. Sun et al., "Bose–Einstein condensation of long-lifetime polaritons in thermal equilibrium", *Phys. Rev. Lett.* **118** (2017), no. 1, article no. 016602.

[48] P. Roushan et al., "Chiral ground-state currents of interacting photons in a synthetic magnetic field", *Nat. Phys.* **13** (2017), no. 2, pp. 146–151.

[49] P. Roushan et al., "Spectroscopic signatures of localization with interacting photons in superconducting qubits", *Science* **358** (2017), no. 6367, pp. 1175–1179.

[50] C. Wang et al., "Realization of fractional quantum Hall state with interacting photons", *Science* **384** (2024), no. 6695, pp. 579–584.

[51] D. F. Walls and G. J. Milburn, *Quantum optics*, Graduate Texts in Physics, Springer, 2008, 425 pages.

[52] C. Ciuti, G. Bastard and I. Carusotto, "Quantum vacuum properties of the intersubband cavity polariton field", *Phys. Rev. B* **72** (2005), article no. 115303.

[53] C. Ciuti and I. Carusotto, "Input-output theory of cavities in the ultrastrong coupling regime: the case of time-independent cavity parameters", *Phys. Rev. A* **74** (2006), article no. 033811.

[54] A. Frisk Kockum, A. Miranowicz, S. De Liberato, S. Savasta and F. Nori, "Ultrastrong coupling between light and matter", *Nat. Rev. Phys.* **1** (2019), no. 1, pp. 19–40.

[55] C. W. Gardiner and P. Zoller, *Quantum noise*, Springer Series in Synergetics, Springer, 2004, xxii+450 pages.

[56] W. E. Lamb, "Theory of an optical maser", *Phys. Rev.* **134** (1964), pp. A1429–A1450.

[57] M. O. Scully and M. S. Zubairy, *Quantum optics*, Cambridge University Press, 1997, xxii+630 pages.

[58] H.-P. Breuer and F. Petruccione, *The theory of open quantum systems*, Oxford University Press, 2002, 648 pages.

[59] J. Lebreuilly, M. Wouters and I. Carusotto, "Towards strongly correlated photons in arrays of dissipative nonlinear cavities under a frequency-dependent incoherent pumping", *C. R. Phys.* **17** (2016), no. 8, pp. 836–860.

[60] T. Becker, L.-N. Wu and A. Eckardt, "Lindbladian approximation beyond ultraweak coupling", *Phys. Rev. E* **104** (2021), article no. 014110.

[61] C. S. Tello Breuer, T. Becker and A. Eckardt, "Benchmarking quantum master equations beyond ultraweak coupling", *Phys. Rev. B* **110** (2024), article no. 064319.

[62] F. Caleffi, M. Capone and I. Carusotto, "Collective excitations of a strongly correlated nonequilibrium photon fluid across the insulator-superfluid phase transition", *Phys. Rev. Lett.* **131** (2023), no. 19, article no. 193604.

[63] E. Kapit, M. Hafezi and S. H. Simon, "Induced self-stabilization in fractional quantum Hall states of light", *Phys. Rev. X* **4** (2014), article no. 031039.

[64] R. Ma, B. Saxberg, C. Owens, N. Leung, Y. Lu, J. Simon and D. I. Schuster, "A dissipatively stabilized Mott insulator of photons", *Nature* **566** (2019), no. 7742, pp. 51–57.

[65] D. Marcos, A. Tomadin, S. Diehl and P. Rabl, "Photon condensation in circuit quantum electrodynamics by engineered dissipation", *New J. Phys.* **14** (2012), no. 5, article no. 055005.

[66] L. Garbe, Y. Minoguchi, J. Huber and P. Rabl, "The bosonic skin effect: boundary condensation in asymmetric transport", *SciPost Phys.* **16** (2024), article no. 029.

[67] F. Petiziol and A. Eckardt, "Cavity-based reservoir engineering for Floquet-engineered superconducting circuits", *Phys. Rev. Lett.* **129** (2022), article no. 233601.

[68] S. Hacohen-Gourgy, V. V. Ramasesh, C. De Grandi, I. Siddiqi and S. M. Girvin, "Cooling and autonomous feedback in a Bose–Hubbard chain with attractive interactions", *Phys. Rev. Lett.* **115** (2015), article no. 240501.

[69] M. Mamaev, L. C. G. Govia and A. A. Clerk, "Dissipative stabilization of entangled cat states using a driven Bose–Hubbard dimer", *Quantum* **2** (2018), article no. 58 (11 pages).

[70] P. M. Harrington, E. J. Mueller and K. W. Murch, "Engineered dissipation for quantum information science", *Nat. Rev. Phys.* **4** (2022), no. 10, pp. 660–671.

[71] Z. Li, T. Roy, Y. Lu, E. Kapit and D. I. Schuster, "Autonomous stabilization with programmable stabilized state", *Nat. Commun.* **15** (2024), article no. 6978 (6 pages).

[72] R. Lescanne et al., "Exponential suppression of bit-flips in a qubit encoded in an oscillator", *Nat. Phys.* **16** (2020), no. 5, pp. 509–513.

[73] L. A. Lugiato, F. Prati, E. Brambilla and A. Gatti, "The cavity Kerr medium model and the surprising history around it", in *Quantum fluids of light and matter*, Proceedings of the International School of Physics "Enrico Fermi", vol. 209, IOS Press, 2025, pp. 5–21.

[74] Y. Castin, "Bose–Einstein condensates in atomic gases: simple theoretical results", in *Coherent atomic matter waves* (R. Kaiser, C. Westbrook and F. David, eds.), EDP Sciences; Springer, 2001, pp. 1–136. Online at https://cel.hal.science/cel-00092947v1. Lecture notes of Les Houches summer school.

[75] M. Wouters and I. Carusotto, "Superfluidity and critical velocities in nonequilibrium Bose–Einstein condensates", *Phys. Rev. Lett.* **105** (2010), no. 2, article no. 020602.

[76] M. C. Cross and P. C. Hohenberg, "Pattern formation outside of equilibrium", *Rev. Mod. Phys.* **65** (1993), no. 3, pp. 851–1112.

[77] I. S. Aranson and L. Kramer, "The world of the complex Ginzburg–Landau equation", *Rev. Mod. Phys.* **74** (2002), no. 1, pp. 99–143.

[78] L. A. Lugiato and R. Lefever, "Spatial dissipative structures in passive optical systems", *Phys. Rev. Lett.* **58** (1987), no. 21, article no. 2209.

[79] I. Carusotto and C. Ciuti, "Spontaneous microcavity-polariton coherence across the parametric threshold: quantum Monte Carlo studies", *Phys. Rev. B* **72** (2005), no. 12, article no. 125335.

[80] M. Wouters and V. Savona, "Stochastic classical field model for polariton condensates", *Phys. Rev. B* **79** (2009), no. 16, article no. 165302.

[81] I. Frérot, A. Vashisht, M. Morassi, A. Lemaître, S. Ravets, J. Bloch, A. Minguzzi and M. Richard, "Bogoliubov excitations driven by thermal lattice phonons in a quantum fluid of light", *Phys. Rev. X* **13** (2023), no. 4, article no. 041058.

[82] M. H. Szymańska, "Stochastic and tensor network methods for open dissipative quantum lattice models", 2025. Talk at the "MEOQS2025 — Methods for many-body open quantum systems" workshop, Trento (2025).

[83] B. Berg, L. I. Plimak, A. Polkovnikov, M. K. Olsen, M. Fleischhauer and W. P. Schleich, "Commuting Heisenberg operators as the quantum response problem: time-normal averages in the truncated Wigner representation", *Phys. Rev. A* **80** (2009), article no. 033624.

[84] A. Sinatra, C. Lobo and Y. Castin, "The truncated Wigner method for Bose-condensed gases: limits of validity and applications", *J. Phys. B. At. Mol. Opt. Phys.* **35** (2002), no. 17, article no. 3599.

[85] M. J. Steel, M. K. Olsen, L. I. Plimak, P. D. Drummond, S. M. Tan, M. J. Collett, D. F. Walls and R. Graham, "Dynamical quantum noise in trapped Bose–Einstein condensates", *Phys. Rev. A* **58** (1998), pp. 4824–4835.

[86] P. D. Drummond, "Quantum optical tunneling: a representation-free theory valid near the state-equation turning points", *Phys. Rev. A* **33** (1986), pp. 4462–4464.

[87] K. Vogel and H. Risken, "Quantum-tunneling rates and stationary solutions in dispersive optical bistability", *Phys. Rev. A* **38** (1988), pp. 2409–2422.

[88] M. Van Regemortel, W. Casteels, I. Carusotto and M. Wouters, "Spontaneous Beliaev–Landau scattering out of equilibrium", *Phys. Rev. A* **96** (2017), no. 5, article no. 053854.

[89] A. Polkovnikov, "Quantum corrections to the dynamics of interacting bosons: beyond the truncated Wigner approximation", *Phys. Rev. A* **68** (2003), no. 5, article no. 053604.

[90] I. Carusotto and C. Ciuti, "Probing microcavity polariton superfluidity through resonant Rayleigh scattering", *Phys. Rev. Lett.* **93** (2004), article no. 166401.

[91] A. Amo et al., "Superfluidity of polaritons in semiconductor microcavities", *Nature Phys.* **5** (2009), no. 11, pp. 805–810.

[92] F. Claude, M. J. Jacquet, R. Usciati, I. Carusotto, É. Giacobino, A. Bramati and Q. Glorieux, "High-resolution coherent probe spectroscopy of a polariton quantum fluid", *Phys. Rev. Lett.* **129** (2022), no. 10, article no. 103601.

[93] X. Busch, I. Carusotto and R. Parentani, "Spectrum and entanglement of phonons in quantum fluids of light", *Phys. Rev. A* **89** (2014), no. 4, article no. 043819.

[94] T. Boulier, E. Cancellieri, N. D. Sangouard, R. Hivet, Q. Glorieux, É. Giacobino and A. Bramati, "Lattices of quantized vortices in polariton superfluids", *C. R. Phys.* **17** (2016), no. 8, pp. 893–907.

[95] C. Barcelo, S. Liberati and M. Visser, "Analogue gravity", *Living Rev. Relativ.* **14** (2011), pp. 1–159.

[96] D. Gerace and I. Carusotto, "Analog Hawking radiation from an acoustic black hole in a flowing polariton superfluid", *Phys. Rev. B* **86** (2012), no. 14, article no. 144505.

[97] H. S. Nguyen et al., "Acoustic black hole in a stationary hydrodynamic flow of microcavity polaritons", *Phys. Rev. Lett.* **114** (2015), no. 3, article no. 036402.

[98] K. Falque, A. Delhom, Q. Glorieux, É. Giacobino, A. Bramati and M. J. Jacquet, "Polariton fluids as quantum field theory simulators on tailored curved spacetimes", *Phys. Rev. Lett.* **135** (2025), article no. 023401 (7 pages).

[99] J. R. Muñoz de Nova, K. Golubkov, V. I. Kolobov and J. Steinhauer, "Observation of thermal Hawking radiation and its temperature in an analogue black hole", *Nature* **569** (2019), no. 7758, pp. 688–691.

[100] S. Finazzi and I. Carusotto, "Entangled phonons in atomic Bose–Einstein condensates", *Phys. Rev. A* **90** (2014), no. 3, article no. 033607.

[101] D. Tong, "Lectures on the quantum Hall effect", preprint, 2016. Online at https://arxiv.org/abs/1606.06687.

[102] T. Ozawa and I. Carusotto, "Anomalous and quantum Hall effects in lossy photonic lattices", *Phys. Rev. Lett.* **112** (2014), no. 13, article no. 133902.

[103] T. Ozawa et al., "Topological photonics", *Rev. Mod. Phys.* **91** (2019), no. 1, article no. 015006.
[104] A. Chénier, B. d'Aligny, F. Pellerin, P.-É. Blanchard, T. Ozawa, I. Carusotto and P. St-Jean, "Quantized Hall drift in a frequency-encoded photonic Chern insulator", preprint, 2024. Online at https://arxiv.org/abs/2412.04347.
[105] I. Carusotto and G. Rousseaux, "The Cerenkov effect revisited: from swimming ducks to zero modes in gravitational analogues", in *Analogue gravity phenomenology: analogue spacetimes and horizons, from theory to experiment*, Lecture Notes in Physics, vol. 870, Springer, 2013, pp. 109–144.
[106] F. Claude, M. J. Jacquet, Q. Glorieux, M. Wouters, É. Giacobino, I. Carusotto and A. Bramati, "Observation of the diffusive Nambu–Goldstone mode of a non-equilibrium phase transition", *Nat. Phys.* **21** (2025), pp. 924–930.
[107] K. Huang, *Statistical mechanics*, John Wiley & Sons, 1987, xiv+498 pages.
[108] M. Richard, J. Kasprzak, R. Romestain, R. Andre and L. S. Dang, "Spontaneous coherent phase transition of polaritons in CdTe microcavities", *Phys. Rev. Lett.* **94** (2005), no. 18, article no. 187401.
[109] M. Wouters, I. Carusotto and C. Ciuti, "Spatial and spectral shape of inhomogeneous nonequilibrium exciton-polariton condensates", *Phys. Rev. B* **77** (2008), article no. 115340.
[110] E. Wertz et al., "Spontaneous formation and optical manipulation of extended polariton condensates", *Nat. Phys.* **6** (2010), no. 11, pp. 860–864.
[111] A. Amo and J. Bloch, "Exciton-polaritons in lattices: a non-linear photonic simulator", *C. R. Phys.* **17** (2016), no. 8, pp. 934–945.
[112] D. Tanese et al., "Polariton condensation in solitonic gap states in a one-dimensional periodic potential", *Nat. Commun.* **4** (2013), no. 1, article no. 1749.
[113] F. Baboux et al., "Unstable and stable regimes of polariton condensation", *Optica* **5** (2018), no. 10, pp. 1163–1170.
[114] D. Nigro, D. Trypogeorgos, A. Gianfrate, D. Sanvitto, I. Carusotto and D. Gerace, "Supersolidity of polariton condensates in photonic crystal waveguides", *Phys. Rev. Lett.* **134** (2025), no. 5, article no. 056002.
[115] D. Trypogeorgos et al., "Emerging supersolidity in photonic-crystal polariton condensates", *Nature* **639** (2025), pp. 337–341.
[116] A. Recati and S. Stringari, "Supersolidity in ultracold dipolar gases", *Nat. Rev. Phys.* **5** (2023), no. 12, pp. 735–743.
[117] S. A. Diddams, K. Vahala and T. Udem, "Optical frequency combs: coherently uniting the electromagnetic spectrum", *Science* **369** (2020), article no. eaay3676 (12 pages).
[118] L. Chang, S. Liu and J. E. Bowers, "Integrated optical frequency comb technologies", *Nature Photon.* **16** (2022), no. 2, pp. 95–108.
[119] D. Bajoni, P. Senellart, A. Lemaître and J. Bloch, "Photon lasing in GaAs microcavity: similarities with a polariton condensate", *Phys. Rev. B* **76** (2007), article no. 201305.
[120] Y. Sun et al., "Bose–Einstein condensation of long-lifetime polaritons in thermal equilibrium", *Phys. Rev. Lett.* **118** (2017), no. 1, article no. 016602.
[121] A. Chiocchetta, A. Gambassi and I. Carusotto, "Laser operation and Bose–Einstein condensation: analogies and differences", in *Universal themes of Bose–Einstein condensation*, Cambridge University Press, 2017, pp. 409–423.
[122] C. Cohen-Tannoudji, "Lectures at Collège de France", 1999-2000. Online at https://www.phys.ens.fr/sites/default/files/2024-03/1999-00.pdf.
[123] S. M. Rezende, *Fundamentals of magnonics*, Lecture Notes in Physics, Springer, 2020, xvii+358 pages.
[124] J. D. Gunton and M. J. Buckingham, "Condensation of the ideal Bose gas as a cooperative transition", *Phys. Rev.* **166** (1968), pp. 152–158.
[125] M. Wouters and I. Carusotto, "Goldstone mode of optical parametric oscillators in planar semiconductor microcavities in the strong-coupling regime", *Phys. Rev. A* **76** (2007), article no. 043807.
[126] R. Graham and H. Haken, "Laserlight–first example of a second-order phase transition far away from thermal equilibrium", *Z. Phys. A, Hadrons Nuclei* **237** (1970), pp. 31–46.
[127] M. Wouters and I. Carusotto, "Absence of long-range coherence in the parametric emission of photonic wires", *Phys. Rev. B* **74** (2006), article no. 245316 (6 pages).
[128] P. Minnhagen, "The two-dimensional Coulomb gas, vortex unbinding, and superfluid-superconducting films", *Rev. Mod. Phys.* **59** (1987), pp. 1001–1066.
[129] Z. Hadzibabic and J. Dalibard, "Two-dimensional Bose fluids: an atomic physics perspective", *Riv. Nuovo Cim.* **34** (2011), no. 6, pp. 389–434.
[130] E. Altman, L. M. Sieberer, L. Chen, S. Diehl and J. Toner, "Two-dimensional superfluidity of exciton polaritons requires strong anisotropy", *Phys. Rev. X* **5** (2015), no. 1, article no. 011017.
[131] L. M. Sieberer, M. Buchhold and S. Diehl, "Keldysh field theory for driven open quantum systems", *Rep. Prog. Phys.* **79** (2016), no. 9, article no. 096001.
[132] A. Zamora, L. M. Sieberer, K. Dunnett, S. Diehl and M. H. Szymańska, "Tuning across universalities with a driven open condensate", *Phys. Rev. X* **7** (2017), no. 4, article no. 041006.
[133] Q. Fontaine et al., "Kardar–Parisi–Zhang universality in a one-dimensional polariton condensate", *Nature* **608** (2022), no. 7924, pp. 687–691.

[134] T. Ozawa, H. M. Price, N. Goldman, O. Zilberberg and I. Carusotto, "Synthetic dimensions in integrated photonics: from optical isolation to four-dimensional quantum Hall physics", *Phys. Rev. A* **93** (2016), no. 4, article no. 043827.

[135] M. Ehrhardt, S. Weidemann, L. J. Maczewsky, M. Heinrich and A. Szameit, "A perspective on synthetic dimensions in photonics", *Laser Photonics Rev.* **17** (2023), no. 7, article no. 2200518.

[136] L. Yuan, Q. Lin, M. Xiao and S. Fan, "Synthetic dimension in photonics", *Optica* **5** (2018), no. 11, pp. 1396–1405.

[137] I. Heckelmann, M. Bertrand, A. Dikopoltsev, M. Beck, G. Scalari and J. Faist, "Quantum walk comb in a fast gain laser", *Science* **382** (2023), no. 6669, pp. 434–438.

[138] A. Dikopoltsev, I. Heckelmann, M. Bertrand, M. Beck, G. Scalari, O. Zilberberg and J. Faist, "Collective quench dynamics of active photonic lattices in synthetic dimensions", *Nat. Phys.* **21** (2025), pp. 1134–1140.

[139] C. J. Flower et al., "Observation of topological frequency combs", *Science* **384** (2024), no. 6702, pp. 1356–1361.

[140] K. A. Takeuchi, "An appetizer to modern developments on the Kardar–Parisi–Zhang universality class", *Phys. A: Stat. Mech. Appl.* **504** (2018), pp. 77–105. Lecture Notes of the 14th International Summer School on Fundamental Problems in Statistical Physics.

[141] K. J. Wiese, "On the perturbation expansion of the KPZ equation", *J. Stat. Phys.* **93** (1998), no. 1, pp. 143–154.

[142] E. Marinari, A. Pagnani and G. Parisi, "Critical exponents of the KPZ equation via multi-surface coding numerical simulations", *J. Phys. A. Math. Gen.* **33** (2000), no. 46, article no. 8181.

[143] L. Canet, H. Chaté, B. Delamotte and N. Wschebor, "Nonperturbative renormalization group for the Kardar–Parisi–Zhang equation", *Phys. Rev. Lett.* **104** (2010), article no. 150601.

[144] A. Imamoğlu, H. Schmidt, G. Woods and M. Deutsch, "Strongly interacting photons in a nonlinear cavity", *Phys. Rev. Lett.* **79** (1997), no. 8, pp. 1467–1470.

[145] I. Carusotto, D. Gerace, H. E. Tureci, S. De Liberato, C. Ciuti and A. Imamoğlu, "Fermionized photons in an array of driven dissipative nonlinear cavities", *Phys. Rev. Lett.* **103** (2009), article no. 033601.

[146] J. R. Johansson, P. D. Nation and F. Nori, "QuTiP: an open-source Python framework for the dynamics of open quantum systems", *Comput. Phys. Commun.* **183** (2012), no. 8, pp. 1760–1772.

[147] Y. Castin, "Simple theoretical tools for low dimension Bose gases", *J. Phy. IV France* **116** (2004), pp. 89–132.

[148] C. Cohen-Tannoudji, J. Dupont-Roc and G. Grynberg, *Atom-photon interactions: basic processes and applications*, Physics Textbook, John Wiley & Sons, 1998, xxii+656 pages.

[149] G. P. Fedorov et al., "Photon transport in a Bose–Hubbard chain of superconducting artificial atoms", *Phys. Rev. Lett.* **126** (2021), article no. 180503.

[150] R. O. Umucalılar and I. Carusotto, "Fractional quantum Hall states of photons in an array of dissipative coupled cavities", *Phys. Rev. Lett.* **108** (2012), article no. 206809.

[151] R. O. Umucalılar and I. Carusotto, "Many-body braiding phases in a rotating strongly correlated photon gas", *Phys. Lett. A* **377** (2013), no. 34–36, pp. 2074–2078.

[152] L. W. Clark, N. Schine, C. Baum, N. Jia and J. Simon, "Observation of Laughlin states made of light", *Nature* **582** (2020), no. 7810, pp. 41–45.

[153] A. V. Gorshkov, J. Otterbach, M. Fleischhauer, T. Pohl and M. D. Lukin, "Photon-photon interactions via Rydberg blockade", *Phys. Rev. Lett.* **107** (2011), article no. 133602.

[154] N. Schine, A. Ryou, A. Gromov, A. Sommer and J. Simon, "Synthetic Landau levels for photons", *Nature* **534** (2016), no. 7609, pp. 671–675.

[155] A. Stern, "Anyons and the quantum Hall effect. A pedagogical review", *Ann. Phys.* **323** (2008), no. 1, pp. 204–249.

[156] B. Paredes, P. Fedichev, J. I. Cirac and P. Zoller, "$\frac{1}{2}$-anyons in small atomic Bose–Einstein condensates", *Phys. Rev. Lett.* **87** (2001), no. 1, article no. 010402.

[157] F. Grusdt, N. Y. Yao, D. Abanin, M. Fleischhauer and E. Demler, "Interferometric measurements of many-body topological invariants using mobile impurities", *Nat. Commun.* **7** (2016), no. 1, article no. 11994.

[158] A. Muñoz de las Heras, E. Macaluso and I. Carusotto, "Anyonic molecules in atomic fractional quantum Hall liquids: a quantitative probe of fractional charge and anyonic statistics", *Phys. Rev. X* **10** (2020), no. 4, article no. 041058.

[159] E. Macaluso and I. Carusotto, "Hard-wall confinement of a fractional quantum Hall liquid", *Phys. Rev. A* **96** (2017), no. 4, article no. 043607.

[160] A. Nardin, D. De Bernardis, R. O. Umucalılar, L. Mazza, M. Rizzi and I. Carusotto, "Quantum nonlinear optics on the edge of a few-particle fractional quantum Hall fluid in a small lattice", *Phys. Rev. Lett.* **133** (2024), no. 18, article no. 183401.

[161] F. Binanti, N. Goldman and C. Repellin, "Spectroscopy of edge and bulk collective modes in fractional Chern insulators", *Phys. Rev. Res.* **6** (2024), article no. L012054 (6 pages).

[162] A. Biella, F. Storme, J. Lebreuilly, D. Rossini, R. Fazio, I. Carusotto and C. Ciuti, "Phase diagram of incoherently driven strongly correlated photonic lattices", *Phys. Rev. A* **96** (2017), no. 2, article no. 023839.

[163] R. O. Umucalılar and I. Carusotto, "Generation and spectroscopic signatures of a fractional quantum Hall liquid of photons in an incoherently pumped optical cavity", *Phys. Rev. A* **96** (2017), no. 5, article no. 053808.

[164] R. O. Umucalılar, J. Simon and I. Carusotto, "Autonomous stabilization of photonic Laughlin states through angular momentum potentials", *Phys. Rev. A* **104** (2021), no. 2, article no. 023704.

[165] P. Kurilovich, V. D. Kurilovich, J. Lebreuilly and S. M. Girvin, "Stabilizing the Laughlin state of light: dynamics of hole fractionalization", *SciPost Phys.* **13** (2022), no. 5, article no. 107 (34 pages).

[166] M. Hafezi, P. Adhikari and J. M. Taylor, "Chemical potential for light by parametric coupling", *Phys. Rev. B* **92** (2015), article no. 174305.

[167] J. Lebreuilly, A. Biella, F. Storme, D. Rossini, R. Fazio, C. Ciuti and I. Carusotto, "Stabilizing strongly correlated photon fluids with non-Markovian reservoirs", *Phys. Rev. A* **96** (2017), no. 3, article no. 033828.

[168] M. J. Jacquet et al., "Quantum vacuum excitation of a quasinormal mode in an analog model of black hole spacetime", *Phys. Rev. Lett.* **130** (2023), no. 11, article no. 111501.

[169] T. Ozawa and H. M. Price, "Topological quantum matter in synthetic dimensions", *Nat. Rev. Phys.* **1** (2019), no. 5, pp. 349–357.

[170] C. Nayak, S. H. Simon, A. Stern, M. Freedman and S. Das Sarma, "Non-Abelian anyons and topological quantum computation", *Rev. Mod. Phys.* **80** (2008), pp. 1083–1159.

[171] T. Tsuno, S. Taie, Y. Takasu, K. Yamashita, T. Ozawa and Y. Takahashi, "Gain engineering and topological atom laser in synthetic dimensions", preprint, 2024. Online at https://arxiv.org/abs/2404.13769.